Polygonal peatlands and treed plateau bog in Northwest Hudson Bay Lowlands, Canada: Holocene development and permafrost dynamics

Tiina H. M. Kolari[a,1], Laure Gandois[b], Frédéric Bouchard[c,d,e], Alison E. Cassidy[f], Nicole K. Sanderson[a,g], Rémi Tremouille[b], Julien Arsenault[h], Maialen Barret[b], Adam Collingwood[f], Lucile Cosyn Wexteen[c,d,e], Sylvain Ferrant[i], LeeAnn Fishback[j], Karen Richardson[f], & Michelle Garneau[a,g]

This is a non-peer-reviewed preprint submitted to EarthArXiv of a manuscript submitted for peer-review to the journal *Quaternary Science Reviews* (17.05.2026).

[a]Research Centre in Earth System Dynamics (GEOTOP), Université du Québec à Montréal, Montréal, QC, Canada
[b]Centre de Recherche sur la Biodiversité et l'Environnement (CRBE), Université de Toulouse, CNRS-UPS-INPT, Toulouse, France
[c]Department of Applied Geomatics & Centre d'applications et de recherche en télédétection (CARTEL), Université de Sherbrooke, Sherbrooke, QC, Canada
[d]Centre d'études nordiques (CEN), Québec, QC, Canada
[e]Groupe de recherche interuniversitaire en limnologie (GRIL), Université de Montréal, Montréal, QC, Canada
[f]Parks Canada, Gatineau, QC, Canada
[g]Département de Géographie, Université du Québec à Montréal, Montréal, QC, Canada
[h]Département des sciences biologiques, Université du Québec à Montréal, Montréal, QC, Canada
[i]Centre d'Etudes Spatiales de la Biosphère (CESBIO), Université de Toulouse, CNES/CNRS/INRAE/IRD/UT3, Toulouse, France
[j]Parks Canada, Churchill, MB, Canada

Corresponding author:
Tiina H. M. Kolari
Email: tiina.kolari@uef.fi
Phone number: +35840 543 9545
[1]Present address: Department of Environmental and Biological Sciences, University of Eastern Finland, Joensuu Campus, Yliopistokatu 7, P. O. Box 111, FI-80101 Joensuu, Finland

Author emails:
LG: laure.gandois@toulouse-inp.fr; FB: frederic.bouchard5@usherbrooke.ca; AEC: alison.cassidy@pc.gc.ca; NKS: sanderson.nicole@uqam.ca; RT: remi.tremouille@utoulouse.fr; JA: arsenault.julien@uqam.ca; MB: maialen.barret@ensat.fr; AC: adam.collingwood@pc.gc.ca; LCW: lucile.cosyn.wexteen@usherbrooke.ca; SF: sylvain.ferrant@idr.fr; LAF: leeann.fishback@pc.gc.ca; KR: karen.richardson@pc.gc.ca; MG: garneau.michelle@uqam.ca

Abstract

Since the retreat of the Laurentide Ice Sheet, peatland development in the Hudson Bay Lowlands (HBL) has been mainly influenced by postglacial isostatic rebound and climate. We studied the timing of permafrost aggradation and the successional trajectories of low Arctic and subarctic polygonal peatlands and a boreal plateau bog in Wapusk National Park (WNP), in northwestern HBL. We also explored the timing of peatland initiation and long-term carbon accumulation between peatland types. Peatland initiation in WNP dates to at least 6000 cal BP, and peat thickness and carbon mass were higher in permafrost peat plateaus (mean: 71.7±21.4 (SE) kg C m^{-2}) and intermediate-centred polygons (63.2±7.14 kg C m^{-2}) than in non-permafrost fens (20.4 ±1.75 kg C m^{-2}). In the boreal plateau bog, permafrost may have been present ~2585–1755 cal BP, while the most recent phase of permafrost aggradation likely occurred at the onset of the Little Ice Age (LIA). In the low Arctic and subarctic polygonal peatlands, permafrost likely developed ~1500–1050 cal BP, during the Dark Ages Cold Period (DACP), suggested by rapid declines in peat and carbon accumulation. In three subarctic sites, dry polygons were preceded by treed *Sphagnum* bogs with *Picea mariana* and *P. glauca*, until spruce disappeared ~1330–780 cal BP. These results suggest that in the subarctic HBL, polygons formed in *Sphagnum*-dominated plateaus after spruce disappeared, during the DACP or at the onset of LIA. In the low Arctic site, dry intermediate-centred polygons formed ~200 cal BP, but the exact successional pathway remained uncertain.

Keywords: age-depth modelling, carbon accumulation, Dark Ages Cold Period, Little Ice Age, permafrost aggradation, plant macrofossils, polygon formation

Highlights

- Permafrost developed in the Dark Ages Cold Period and the Little Ice Age
- Sharp declines in peat accumulation best indicated permafrost aggradation
- Development history differed between low Arctic and subarctic polygons
- In subarctic tundra, treed *Sphagnum* bogs preceded dry ice-wedge polygons
- In the low Arctic site, wet fens preceded dry polygons until the end of the LIA

Introduction

Northern peatlands store 415 ± 150 Pg of carbon (C), of which approximately half is found in permafrost regions (Hugelius et al., 2020). Currently, the Arctic is warming almost four times faster than the rest of the globe (Rantanen et al., 2022), resulting in frozen ground temperatures and active layer thicknesses increasing across the Arctic (Biskaborn et al., 2019; Langer et al., 2024; Smith et al., 2022), and posing a threat to the C stored in permafrost (Hugelius et al., 2020; Schuur et al., 2015, 2022; Treat et al., 2021). Many continuous permafrost regions are characterized by ice-wedge polygon peatlands, where permafrost thaw can cause variable changes in peatland microtopography, hydrology, and vegetation (Jorgenson et al., 2006; 2022; Parmentier et al., 2014; Wolter et al., 2016, 2018). These changes range from the collapse of large ice wedges and the formation of thermokarst ponds with an increase in aquatic vegetation (Jorgenson et al., 2006, 2022) to lake desiccation (Bouchard et al., 2013; Webb et al., 2022) and the creation of dry elevated polygon centres with increasing cover of lichens and shrubs (Liljedahl et al., 2016; Wolter et al., 2016, 2018).

To better understand these landscape-level changes and predict future responses to ongoing warming, it is important to consider how polygonal peatlands typically form, and how that connects to permafrost aggradation and degradation. It is known that ice-wedge polygons form through thermal contraction cracking of frozen peat or mineral soil in high-latitude areas; extreme winter temperatures, high winds, and thin snow cover allow the ground to cool rapidly and crack (Mackay, 1993; Fortier & Allard, 2005; Kokelj et al., 2014). The cracks fill with water from snowmelt in spring and summer, forming ice wedges when the water freezes immediately below the active layer and later in winter within the active layer (Mackay, 2000). Over several annual freeze–thaw cycles, the wedges expand vertically and laterally, creating a network of either low-, intermediate-, or high-centred ice-wedge polygons. In terms of vegetation, low-centred polygons are typically dominated by fen vegetation (sedges and mosses of wet habitats), while lichens and dwarf shrubs are abundant on the dry surfaces of intermediate- and high-centred polygons (Mackay, 2000; Wolter et al., 2016). Low-centred polygons often form on newly exposed mineral soil in coastal lowlands or drained lakes and can evolve into intermediate-centred polygons through peat accumulation in the shallow polygons/pools (Mackay, 2000) or through ice wedge degradation (Liljedahl et al., 2016). Eventually, intermediate-centred polygons can develop rapidly into high-centred polygons

through further ice-wedge degradation and deepening of water-filled troughs surrounding the polygons (Abolt et al., 2020; Kanevskiy et al., 2017; Liljedahl et al., 2016; Wolter et al., 2018). However, the exact pathways can depend on local hydrology, climate, and vegetation (De Klerk et al., 2011; Ellis et al., 2008; Parmentier et al., 2024; Payette et al., 1986; Wolter et al., 2018).

Polygon-forming processes are particularly important in northwestern regions of Hudson Bay Lowlands (HBL). The entire HBL peatland complex is the second largest in the world, with an estimated C storage of ~30 Pg (Li et al., 2025). Currently, the extensive polygonal peatlands in the northwestern HBL are mostly lichen-dominated and intermediate-centred. It is unknown, however, whether these dry polygons have formed rapidly from wet polygons during the past decades or century, in response to ongoing warming and ice-wedge degradation, as reported from the Low and High Arctic regions (Abolt et al., 2020; Kanevskiy et al., 2017; Liljedahl et al., 2016; Wolter et al., 2018), or whether their formation is climate-driven by long-term (centennial- to millennial-scale) dynamics. For example, some evidence exists that in subarctic regions, ice-wedges and dry polygons could also form in relatively dry conditions after natural tree removal (Payette et al., 1986), instead of evolving from wet, low-centred polygons. A comprehensive understanding of the Holocene history of the polygonal peatlands in the northwestern HBL is crucial, particularly, to accurately estimate the fate of vast C storage under warming and increased microbial activity (Kirkwood et al., 2021; Schuur et al., 2015, 2022; Treat et al., 2021).

In this study, we explored Holocene peatland development and permafrost dynamics in four dry, intermediate-centred polygonal peatlands and one treed plateau bog in the northwestern HBL. We collected peat profiles for paleoecological reconstructions across three different vegetation zones (low Arctic and subarctic tundra, and northern boreal forest) in Wapusk National Park (WNP) and the Churchill Wildlife Management Area. In the northern HBL, the Holocene development of permafrost peatlands has been previously studied by Dredge & Mott (2003) and Kuhry (2008). These studies mainly focused on treed/forested plateau bogs in the boreal forest along the Hudson Bay railroad south of Churchill (Manitoba), where land emerged from the sea between 7800 and 6800 ^{14}C yr BP (Dredge & Mott 2003), and peatland initiation followed paludification of upland forests (Kuhry 2008). Using pollen analysis, Dredge & Mott (2003) concluded that vegetation has been relatively stable over the

past six millennia, characterized by *Sphagnum fuscum* and *Picea mariana*. However, little is known about the development of polygonal peatlands in this region.

Specifically, our research questions were: 1) When did permafrost aggradation occur across different vegetation zones (low Arctic tundra, subarctic tundra, and northern boreal forest), 2) have permafrost conditions remained stable throughout the Holocene, and 3) did intermediate-centred polygons evolve from low-centred polygons, and does the successional trajectory differ between vegetation zones? During field campaigns, large pieces of wood were found in permafrost peat cores, and small tree trunks have also been found at the bottom of the shallow lakes in WNP. Therefore, we also asked whether the polygonal peatlands were treed/forested before the formation of the polygons and, if so, what factors led to the disappearance of the trees? Furthermore, we explored the timing of peatland initiation and long-term (centennial- and millennial-scale) carbon accumulation in permafrost peatlands and non-permafrost fens across the region.

2 Materials and Methods

2.1 Study area and sites

This study was conducted in Wapusk National Park (WNP) and the Churchill Wildlife Management Area, located along the western coast of Hudson Bay, near Churchill (58° 46' 09" N, 94° 10' 09" W) in northern Manitoba, Canada (**Figure 1**). WNP covers 11 475 km^2. The region was covered by the Laurentide Ice Sheet until ~8.5 ka BP, and the postglacial Tyrell Sea transgressed over the area by ~8.1 ka BP (Gauthier et al., 2020; Dalton et al., 2023). Since then, peatland development has been largely driven by glacial isostatic adjustment (GIA), with a present-day uplift rate of ~10 mm a^{-1} (Sella et al., 2007), and recession of the Tyrell Sea (Dredge & Mott, 2003; Glaser et al., 2004; Packalen et al., 2014).

The study area is located within both continuous and discontinuous permafrost (Obu et al., 2019). In 1991–2020, mean annual average air temperature (MAAT) in Churchill was -6.0°C, and mean annual precipitation sum was 447.7 mm (Environment and Climate Change Canada, *open data)*. The mean daily average temperature (°C) of the coldest month (January) was -25.3, and that of the warmest month (July) was 13.0. WNP spans over three vegetation zones from southwest to northeast: northern boreal woodland, subarctic woodland-tundra,

and low arctic shrub tundra (Baldwin et al., 2020). Hereafter, we refer to these zones as boreal forest, subarctic tundra, and low Arctic tundra, respectively.

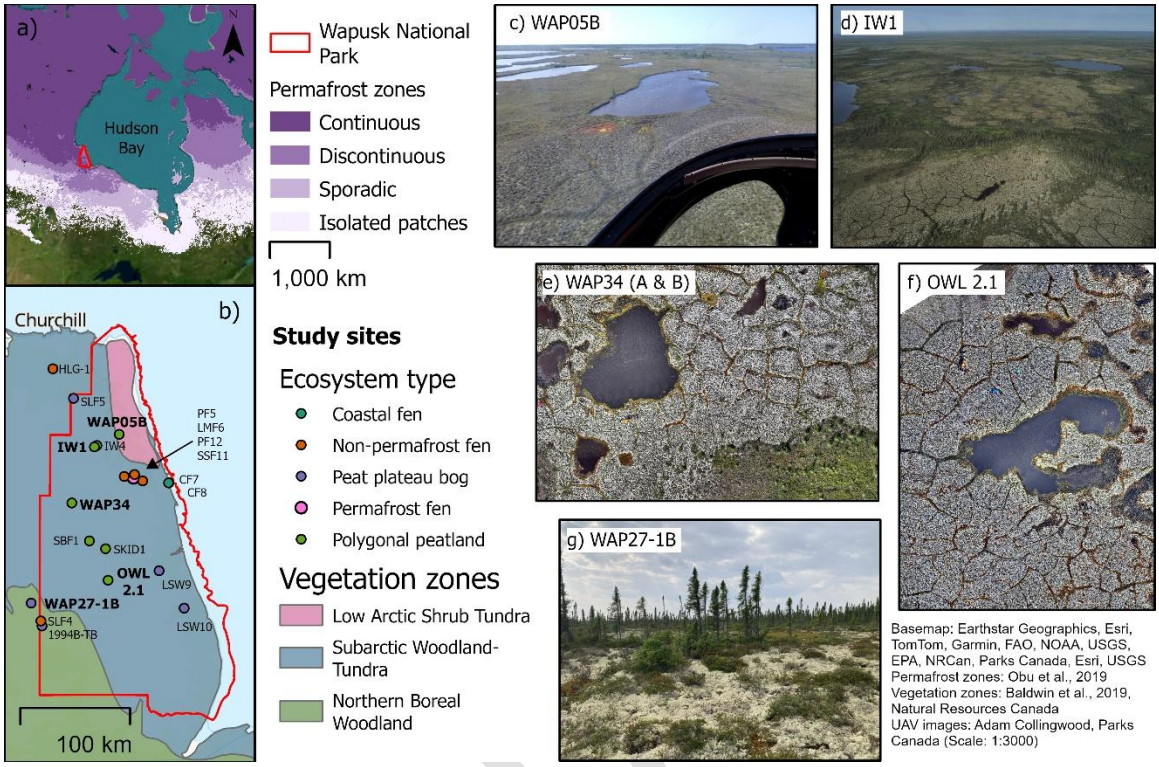

Figure 1. Study area and peat coring locations. Location of Wapusk National Park (WNP) in northwestern Hudson Bay Lowlands (a) and peat coring locations in WNP and Churchill Wildlife Management Area, across Low Arctic Shrub Tundra, Subarctic Woodland-Tundra, and Northern Boreal Woodland zones (b). Photos and UAV images are presented for paleoreconstruction sites: low Arctic polygonal peatland WAP05B (c), subarctic polygonal peatlands IW1 (d), WAP34 (e), OWL 2.1 (f), and a treed plateau bog WAP27-1B (g). At the WAP34 site, peat cores were collected from both polygon centre (A) and ice-wedge trough (B). The map contains information licensed under the Open Government Licence – Canada.

A total of 21 peat profiles were collected between 2023 and 2025 (**Figure 1**; **Supplemental Table S1**). Peat coring locations were preliminarily selected based on satellite imagery, the Wapusk ecotype map report (Pomonorenko et al., 2014), and helicopter aerial surveys. The aim was to cover all types of permafrost and non-permafrost peatlands described by Pomonorenko et al. (2014). Moreover, an effort was made to sample near one pond/lake in each vegetation zone, as included in the ecological integrity monitoring program for Wapusk National Park (lakes WAP05 in low Arctic tundra, WAP34 in subarctic tundra, and WAP27 in northern boreal forest).

2.1.1 Sites for paleoecological reconstructions

Peat profiles for detailed paleoecological reconstructions were collected from four polygon centres (WAP05B, WAP34A, OWL2.1, and IW1) and one treed peat plateau (WAP27-1B), representing the three vegetation zones (**Figure 1**). At the WAP34 site, a peat core was also collected from an ice-wedge trough (WAP34B) for radiocarbon (^{14}C) dating (see section 2.4).

Most polygons in this region are intermediate-centred, and they are characterized by the dominance of *Cladonia* lichens, particularly *C. arbuscula, C. rangiferina*, and *C. stellaris*. Although some ice-wedge degradation was observed, it is noteworthy that most ice-wedge troughs were only slightly lower than polygon centres, and that they were not water-filled. Instead, hummock-level *Sphagnum* moss species (mainly *S. fuscum*) were abundant in the troughs. Of dwarf shrubs, *Empetrum nigrum* and *Rhododendron tomentosum* were common both on polygon centres and troughs, particularly at the WAP05 site. Treed peat plateaus are dominated by *C. stellaris, Picea glauca*, and *P. mariana*.

The active layer thickness (ALT) was 50 cm at the treed plateau (WAP27-1B), 56 cm at the ice-wedge trough (WAP34B) and ranged from 32 to 45 in polygon centres. The measurements were taken either in mid-July 2024 or mid-August 2023, while the maximum ALT is reached in late August or September.

2.1.2 Sites for estimating peatland initiation and carbon accumulation across the region

To estimate the timing of peatland initiation, total carbon masses, and long-term apparent rates of carbon accumulation (LORCA) across the study region, we collected 15 additional peat profiles **(Figure 1; Supplemental Table S1)**, spanning from the subarctic coastal fens to the boreal forest and corresponding to all permafrost and non-permafrost peatland types described by Pomonorenko et al. (2014), except for *Sphagnum* poor fens. Permafrost sites comprised three polygonal peatlands, four treed/forested plateau bogs, and an open rich fen. Non-permafrost sites comprised a treed bog, a treed rich fen, three open rich fens, two coastal fens, and a poor shrub-sedge fen.

2.2 Field sampling

Fieldwork was mainly conducted during the 2023–2025 growing seasons, with two peat profiles collected in March 2025 (**Supplemental Table S1**). At permafrost sites, the peat from the active layer was collected into metal boxes (30 × 12 × 6 cm or 50 × 12 × 6 cm). Beneath the active layer, frozen cores were retrieved using a SIPRE permafrost corer outfitted with a 7.62 cm core barrel. In non-permafrost fens, peat cores were only collected in metal boxes, as the peat thickness did not exceed 51 cm over mineral soil. Cores were kept at -20°C until analyses.

2.3 Laboratory analyses

2.3.1 Bulk density, total organic carbon content, and C/N ratio

All peat cores were sliced into 1-cm sections using a serrated knife. Permafrost cores were cut after thawing at 4 °C for 3-7 days or at room temperature overnight, preferably when they were still icy but easy to slice. No permafrost cores had segregated ice lenses (**Supplemental Figures S1-S5**), and the length of each core was measured frozen and after thawing, to estimate potential water loss and compression. On average, the difference between frozen and thawed length was 1 cm (0-2.5 cm). This compression was considered to have a limited effect on subsequent analyses.

The total organic matter content was analyzed using the loss-on-ignition method (LOI; Chambers et al., 2011), with contiguous 1-cm intervals for paleoreconstruction sites and contiguous 3-cm sections for other sites. For each 1- or 3-cm layer, a 3 cm^3 peat sample was weighed and dried at 105 °C overnight to determine the dry bulk density (g cm^{-3}). The dried samples were burned at 550 °C for three hours to determine organic matter content (%) and to calculate organic matter density (g cm^{-3}). Organic C density (g cm^{-3}) was calculated by multiplying the total organic matter density by 0.5 (Turunen et al., 2002).

For WAP27-1B and OWL 2.1 cores, total carbon and nitrogen (N) contents (%) were analyzed at 2-cm intervals to calculate the C/N ratio. Prior to analysis, peat samples of ca. 2 cm^3 were dried at 60 °C for approximately 48 hours and then ground using a mortar and pestle. Subsequently, subsamples of 1.5–2.2 mg of dried peat were analyzed for C and N using an Elementar Vario MicroCube analyzer at the light stable isotope geochemistry laboratory at

Geotop-UQAM in Montreal, Canada. For WAP05B and WAP34A, C and N contents (%) were analyzed from paired profiles collected during the same day, less than 1 m apart. The paired profiles were analyzed for C% and N% in 5-cm sections at the PAPC (CRBE laboratory, Toulouse, France) on 15 to 20 mg subsamples, using an elemental analyzer ThermoScientific, Flash 2000, and NCS FC and Soil CNS Reference as certified materials.

2.3.2 Plant macrofossils

Peat profiles for paleoecological reconstructions were analyzed for plant macrofossil composition at 4 cm intervals. Macrofossil composition was determined from 3 cm^3 peat samples, which were pre-treated following the protocol of Mauquoy et al. (2010), with some minor adjustments. Peat samples were first gently boiled in a 5% KOH solution for 5-10 minutes, then rinsed with distilled water and sieved through a 125 µm sieve. The abundance of plant macrofossil groups (*Sphagnum* mosses, brown mosses, herbaceous, ligneous, and lichens) was estimated in percentages using a stereoscopic microscope. Coniferous needles, ericaceous leaves, Cyperaceae seeds and rhizomes, charcoal fragments, Chironomidae head capsules, *Daphnia* resting eggs (ephippia), and Oribatid mites were counted. When possible, brown mosses were identified to the species level, following Faubert (2014). *Sphagnum* mosses were identified to section, aggregate, or species level by checking 50 random *Sphagnum* branch leaves with a light microscope, following Laine et al. (2009) and Ayoutte & Rochefort (2019). Leaf counts were converted to percentages, with one leaf representing 2% of the total abundance of *Sphagnum* mosses. They were identified to species level only when stem leaves were also present. Nomenclature of all species follows Global Biodiversity Information Facility (www.gbif.org, accessed November 20th, 2025).

Plant macrofossil diagrams were created using the *riojaPlo*t package (Juggins, 2025) in R version 4.5.1 (R Core Team, 2025). Taxa that reached at least 5 or 6% in abundance or countable macrofossils that appeared at least three or five times (depending on the core) are included in the diagrams. Different zones in peat profiles were identified using constrained incremental sum of squares hierarchical clustering (CONISS) and the function chclust in the *rioja* package (Juggins, 2024). CONISS was performed with surface lichens, except for WAP05B, where dwarf shrubs dominate contemporary vegetation. Surface vegetation is not commonly included in macrofossil diagrams, and lichens tend to decompose rapidly (Harris

et al., 2018). Still, in our opinion, it is crucial to recognize the contemporary lichen-dominated phase from the preceding one in the profiles.

2.4 ^{14}C dating and chronologies

A total of 43 samples were submitted to the A.E. Lalonde AMS Laboratory (University of Ottawa, Canada) for radiocarbon (^{14}C) dating. The basal age of each core and the major transitions in plant macrofossil assemblages were dated for paleoreconstructions. *Sphagnum* moss stems were preferably selected for dating. Ericaceous leaves, coniferous needles, moss stems, and Cyperaceae seeds were selected when *Sphagnum* stems were not sufficiently abundant. Two charcoal samples were submitted to date wildfires at the WAP27-1B site. In addition, eight bulk peat samples were selected when the basal peat was highly decomposed or comprised mainly of Cyperaceae tissue and rootlets. Radiocarbon dates were calibrated (cal BP) using the IntCal20 calibration curve (Reimer et al., 2020).

Bayesian age-depth models were performed for paleoreconstructions using the R package *rbacon* version 3.5.2 (Blaauw & Christen, 2011) in R version 4.5.1 (R Core Team, 2025). Dates were modelled (cal BP) in *Bacon* using the IntCal20 calibration curve (Reimer et al., 2020). The surface of the peat cores was set at -73 or -74 cal BP, corresponding to 2023 and 2024 when the cores were collected, with 0 representing 1950 CE. Age-depth models are available as supplementary material (**Figures S6-S10**).

2.5 Peat and carbon accumulation

Peat accumulation rate (PAR; mm a^{-1}) and long-term apparent rate of carbon accumulation (LORCA, g C m^{-2} a^{-1}) were calculated for all 20 sites (excluding the WAP34B ice wedge) by dividing the peat thickness and total carbon mass by the basal ^{14}C calibrated median age. As point age estimates don't represent the uncertainties involved in ^{14}C dating (Millard, 2014), PAR and LORCA ranges, calculated using the entire age probability ranges, are presented for each site in **Supplementary Table S2**.

For each zone identified in paleoreconstruction peat profiles, PAR and carbon accumulation rates (CAR; g C m^{-2} a^{-1}) were calculated by dividing the peat layer thickness and carbon mass

by the deposition time (yr/cm) obtained by the Bacon age-depth models. 95% confidence intervals for the start and end of each zone, as well as PAR and CAR ranges for all zones, are found in **Supplementary Table S3.**

3 Results

3.1 Peatland initiation across WNP

In the boreal forest, peat accumulation began during the Mid-Holocene. The deepest and the oldest peat deposit (2.6 m) was found at the treed plateau 1994B-TB (**Figure** 1), where peat started to accumulate approximately 6000 cal BP (**Tables 1 and 2**). At the polygonal peatlands in the subarctic tundra, peat accumulation began during the Late Holocene, ~3705–3215 cal BP. The polygonal peatland WAP05B had a younger basal age of 2400 cal BP, which is consistent with its location closer to the coast in the low Arctic tundra zone. Site SKID1 is a polygonal peatland located in the subarctic tundra, but close to Skidmore Lake, where peat accumulation started even later, roughly 1460 cal BP. The basal ages of subarctic treed and forested peat plateaus (LSW9, LSW10, and SLF5) ranged from 1730 to 405 cal BP. At subarctic non-permafrost fens (LMF6, SSF11, and PF12), peat accumulation began ~2155–1255 cal BP. The basal ages of subarctic coastal fens (CF7 and CF8) were each ~30–260 cal BP (1690–1920 CE); this wide range reflects the reduced chronological precision due the Seuss effect and complexities in radiocarbon calibration (Reimer et al., 2020).

3.2 Long-term peat and carbon accumulation across WNP

On average, the highest peat and carbon accumulation rates were found in treed/forested plateau bogs (n = 5), with a mean PAR of 0.73±0.23 (SE) mm a^{-1}, a mean carbon mass of 71.7±21.4 (SE) kg C m^{-2}, and a mean LORCA of 37.8±13.0 (SE) g C m^{-2} a^{-1}. LORCA ranged from 20.6 to 36.9 g C m^{-2} a^{-1}, except for LSW10, with LORCA of 88.4 g C m^{-2} a^{-1} (**Table 2**). It is noteworthy, however, that the LSW10 site was the youngest of the peat plateaus, with a basal age of ~405 cal BP. In polygonal peatlands (n = 7), mean PAR was 0.41±0.04 (SE) mm a^{-1}, mean carbon mass 63.2±7.14 (SE) kg m^{-2}, and mean LORCA 22.0±3.03 (SE) g C m^{-2} a^{-1}. In non-permafrost fens (n = 5), mean PAR was 0.26±0.05 (SE) mm a^{-1}, mean carbon mass 20.4 ±1.75

(SE) kg m^{-2}, and mean LORCA 12.7 (SE ±1.64) g C m^{-2} a^{-1}. The subarctic coastal fens, CF7 and CF8, had relatively high LORCA values of 71.9 and 113.3 g C m^{-2} a^{-1}, respectively, reflecting their young age (~30–260 cal BP) and incompletely decomposed peat. Also, the wide age range for CF7 and CF8 increases the uncertainty in both PAR and LORCA (**Table S2**).

3.3 Peat C and N content (%) and C/N ratio

Across four permafrost peat cores, the median C content was 43.5% (IQR 42.2–44.7%), the median N content was 0.96% (IQR 0.62–2.0%), and the median C/N ratio was 45.3 (IQR 20.2–68.2). N content declined, and the C/N ratio increased with the shift from fen to *Sphagnum* moss-dominated bog vegetation (**Figures 2-6**). Across sites, the highest median %N was found at WAP05B (2.24%) and the lowest at WAP34A (0.77%).

Median C contents did not differ between active layer and permafrost peat (43.3% and 43.6%, respectively), but median N content was lower in active layer peat (0.74%, IQR 0.43–1.10%) than in permafrost peat (1.02%, IQR 0.68–2.11%). Correspondingly, the median C/N ratio was higher in active layer peat (58.7, IQR 40.4–92.0) than in permafrost peat (43.5, IQR 18.9–63.5).

3.4 Paleoecological reconstructions of permafrost peatlands

3.4.1 Low Arctic tundra

At WAP05B polygonal peatland, peat thickness was 110 cm, and PAR was 0.46 mm a^{-1} (**Table 2**). Peat started to accumulate ~2400 cal BP (**Tables 2 and 3**), and four main zones were identified in the plant macrofossil assemblages (**Figure 2**). WAP05B began to develop over newly exposed mineral soil as a rich fen characterized by *Tomentypnum nitens* (zone 1; 2400–2000 cal BP), followed by two fen phases (zones 2a and 2b) characterized by Cyperaceae sedges and mosses of the family Calliergonaceae. The presence of *Scorpidium scorpioides* (zone 2a; 2000–1100 cal BP) and Chironomidae head capsules and *Daphnia* eggs (zone 2b, 1100–200 cal BP) suggests wetter conditions than during the initial *T. nitens* rich-fen phase. The most recent fen phase (2b) lasted until ~200 cal BP, when bog mosses *Aulacomnium* sp.,

Dicranum sp., and *Hylocomnium splendens* took over. This rapid transition to drier bog vegetation suggests the formation of dry, intermediate-centred polygons during the Little Ice Age (LIA). On average, both the highest PAR (0.67 mm a^{-1}) and CAR (51.9 g C m^{-2} a^{-1}) were recorded in zone 3 (200 cal BP to the present; **Table 4**), which corresponds to the most recent, poorly decomposed peat (Young et al., 2019). The median N content (%) was lowest (0.94%) and the C/N ratio highest (45.9) in zone 3.

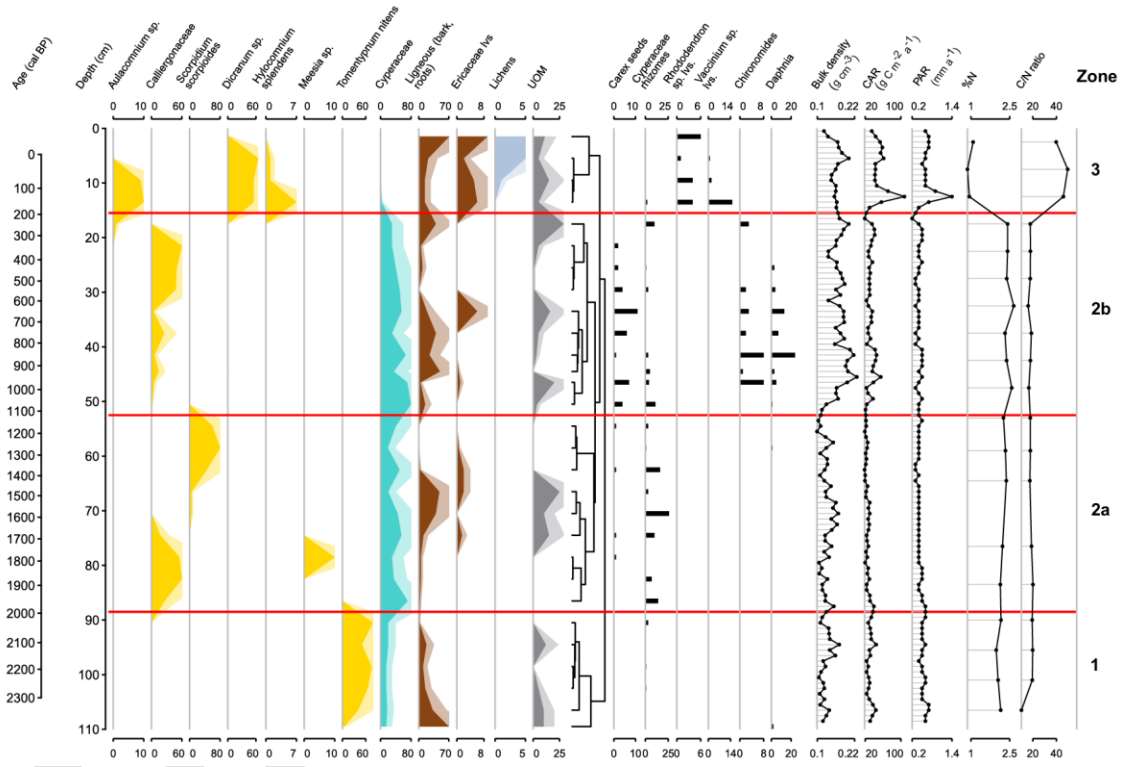

Figure 2. Low Arctic polygon WAP05B. Plant macrofossil abundances (%) and counts, bulk density, carbon (CAR) and peat (PAR) accumulation rates, and peat N content (%) and C/N ratio for WAP05B. Different zones in the peat profile were identified using constrained hierarchical clustering (CONISS).

3.4.2 Subarctic tundra

All paleoreconstruction sites in this region were polygonal peatlands, where peat started to accumulate between ~3700 and 3550 cal BP (**Tables 2 and 3**).

At IW1, peat thickness was 105 cm. Peat accumulation started ~3565 cal BP, and PAR was 0.29 mm a^{-1}. Ligneous and herbaceous rootlets characterized zone 1 (3565–2680cal BP; **Figure 3**). The occurrence of *Sphagnum* cf. *capillifolium* and *Vaccinium oxycoccos* leaves

suggests that bog development began during this initial phase. From ~2680 to 2180 cal BP (zone 2), the high abundance of *Sphagnum fuscum* and *Picea mariana* needles indicates a treed bog phase. The decreased abundance of *S. fuscum* and increased abundance of ligneous material from 59 to 46 cm (zone 3a; 2180–1775 cal BP) suggests a forested phase with *P. mariana*. From 1775 to 800 cal BP (zone 3b), the site was still dominated by *S. fuscum,* but *P. mariana* disappeared ~1330 cal BP. Peat accumulation diminished ~1050 cal BP, potentially suggesting shorter growing seasons and permafrost aggradation. The presence of charcoal between 8 and 3 cm below the surface suggests a local fire between ~860 and 250 cal BP. Zone 3c (~800-present) was characterized by *Cladonia* lichens. The highest PAR values were recorded in zones 2 and 3b, both characterized by *S. fuscum* and *P. mariana,* while the highest CAR (19.8 g C m^{-2} a^{-1}) was recorded in zone 3a.

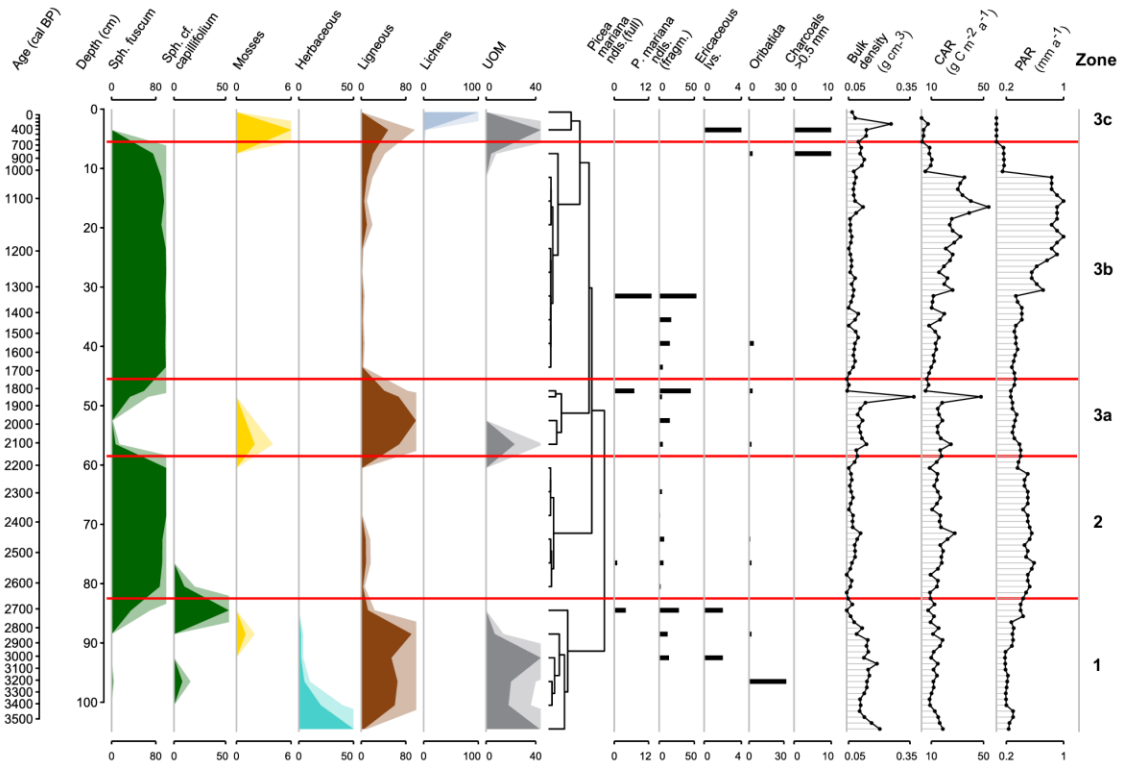

Figure 3. Subarctic polygon IW1. Plant macrofossil abundances (%) and counts, bulk density, and carbon (CAR) and peat (PAR) accumulation rates for IW1. Different zones in the peat profile were identified using constrained hierarchical clustering (CONISS).

At WAP34A, peat thickness was 180 cm, and PAR was 0.51 mm a^{-1} (**Table 2**). Peat accumulation began ~3550 cal BP, and five main phases were identified (**Figure 4; Table 4**). Until ~3150 cal BP (zone 1a), the site was a sedge-dominated fen or a swamp with

shrubs/trees of the Betulaceae family (birch and/or alder). Between ~3150 and 1800 cal BP (zone 1b), the WAP34A site was characterized by coniferous trees and herbaceous vegetation. Initially, *Larix* co-occurred with Betulaceae species, followed by the appearance of *Picea mariana* and *Pleurozium schreberi* ~2300 cal BP. The appearance of *P. mariana* also coincided with the emergence of the first *Sphagnum* mosses (section Acutifolia). From ~1800 to 1460 cal BP (zone 2a), vegetation was dominated by *S. fuscum* type and *Vaccinium oxycoccos*, indicating an open bog phase. Peat and carbon accumulation rates were the highest during this open bog phase, with reconstructed PAR of 1.31 mm a^{-1} and CAR of 43.4 g C m^{-2} a^{-}1, while median N content (%) was the lowest (**Table 4**). The zone 2b (from 1460 to 550 cal BP) remained dominated by *S. fuscum* type, though the abundance of *P. mariana* needles suggests a treed bog phase. Peat accumulation decreased ~1265 cal BP, indicating permafrost aggradation, and *S. fuscum* type and *P. mariana* completely disappeared ~780 cal BP. The vegetation shifted to dominance by tundra mosses, including *S. lenense* and *Dicranum* spp., ~550 cal BP (zone 2c). Correspondingly, the basal age of the peat core from an ice-wedge through (WAP34B) was ~570 cal BP, suggesting that polygonal features started to form ~600–500 cal BP.

At OWL2.1, peat thickness was 166 cm, and PAR was 0.45 mm a^{-1} (**Table 2**). Peat accumulation began ~3700 cal BP. The beginning of zone 1a (3700–2700 cal BP) was characterized by sedges and *Scorpidium scorpioides*, indicating wet conditions of a moderately rich fen. Bog species, including *Picea mariana* and *Chamaedaphne calyculata*, appeared ~3200 cal BP. Between 2700 and 2200 cal BP (zone 1b), OWL2.1 was characterized by *Sphagnum* sect. *Acutifolia*, *Vaccinium oxycoccos*, and *P. mariana*, representing a treed bog phase. The highest PAR (1.04 mm a^{-1}) and CAR (30.6 g C m^{-2} a^{-1}) were recorded for zone 1b (**Table 4**). *Larix laricina* needles increased towards the end of zone 1b. From 2200 to 500 cal BP (zone 2a), the site remained dominated by *Sphagnum* mosses and *P. mariana*, but species of *Sphagnum* sect. *Cuspidata* were also abundant. The peat accumulation rate decreased ~1500 cal BP, suggesting permafrost aggradation. *P. mariana* needles were not found above 30-31 cm, dating ~890 cal BP. Some charcoals were found in the same layer, followed by a peak in wet-habitat species *Warnstorfia fluitans* aggr., suggesting that the fire event may have triggered permafrost thaw. Ligneous rootlets and bark, as well as remnants of lichens, peaked at 22 cm depth (~270 cal BP), possibly linked with a second phase of

426 permafrost aggradation. From 400 cal BP to the present (zone 2b), OWL2.1 was dominated
427 by a tundra species, *Sphagnum lenense*, until lichens took over in the 20th century.

428

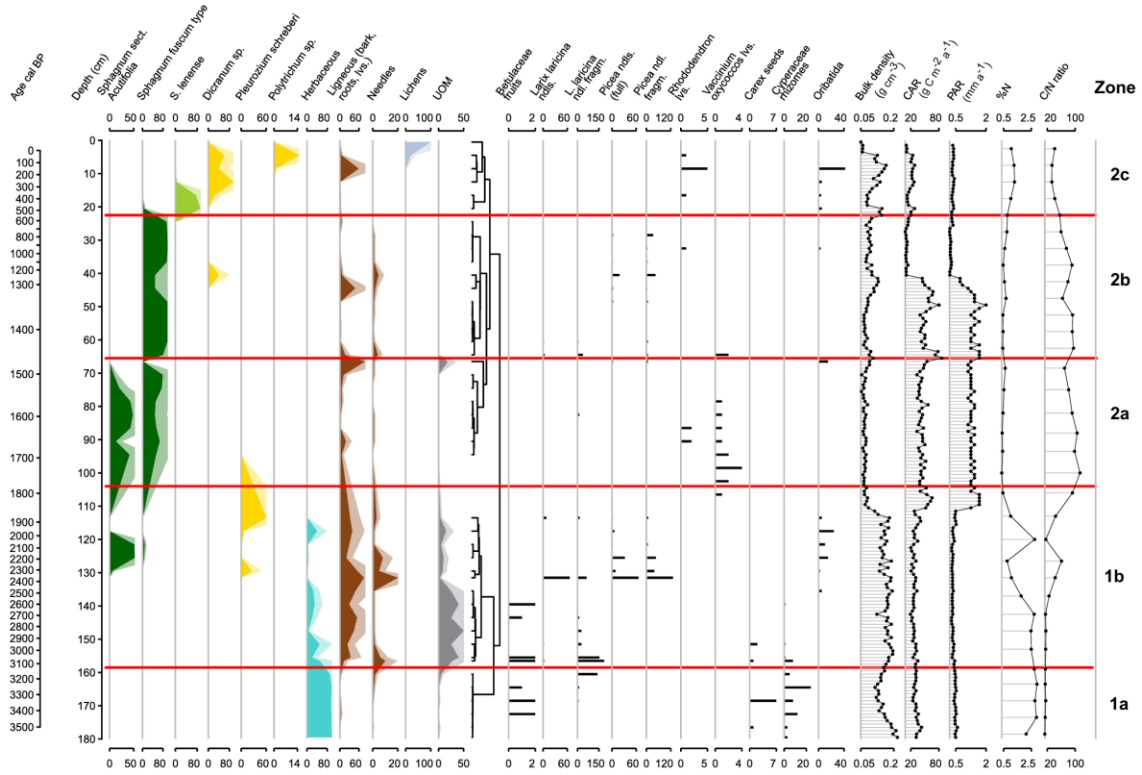

429

430 **Figure 4.** Subarctic polygon WAP34A. Plant macrofossil abundances (%) and counts, bulk density,
431 carbon (CAR) and peat (PAR) accumulation rates, and peat N content (%) and C/N ratio for WAP34A.
432 Different zones in the peat profiles were identified using constrained hierarchical clustering (CONISS).

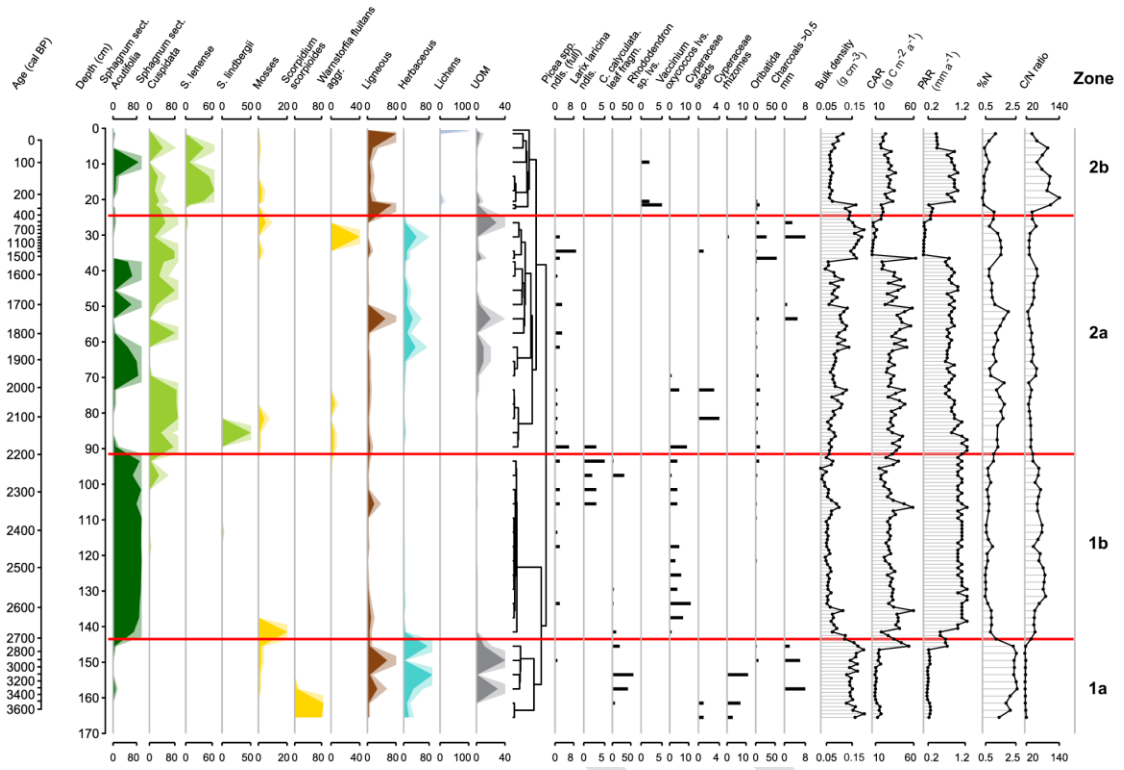

Figure 5. Subarctic polygon OWL 2.1. Plant macrofossil abundances (%) and counts, bulk density, carbon (CAR) and peat (PAR) accumulation rates, and peat N content (%) and C/N ratio for OWL 2.1. Different zones in the peat profile were identified using constrained hierarchical clustering (CONISS).

3.4.3 Northern boreal forest

At WAP27-1B peat plateau bog, peat thickness was 251 cm, and PAR was 0.44 mm a^{-1} (**Table 2**). Peatland initiation began ~5700 cal BP. However, the base of the core (286–251cm) was characterized by fluctuating layers of mineral soil and organic matter, likely reflecting glacial isostatic adjustment and sea-level fluctuations (Dalton et al. 2023; Gauthier et al., 2020). Between 5700 and 3800 cal BP (zone 1a), plant macrofossils were characterized by Betulaceae leaves and fruits, *Carex* and *Juncus* seeds, Cyperaceae rhizomes, and *Daphnia* eggs (**Figure 6**). This indicates a shrub-sedge fen phase with high water table. Calliergonaceae mosses, *Myrica gale* leaves, and *Larix laricina* needles increased towards the end of this phase.

Sphagnum sect. *Acutifolia* and *Picea mariana* appeared ~3700 cal BP, characterizing zone 1b (3800–2600 cal BP). Charred *Picea* needles and charcoals were also abundant, indicating at least one wildfire ~2750 cal BP (**Table 3**). After the fire, the site was still characterized by

Sphagnum fuscum, and *P. mariana* increased over time (zone 1c; ~2600–1600 cal BP). In contrast to the subarctic sites, peat accumulation was the lowest during this treed bog phase (PAR = 0.23 mm a^{-1}; **Table 4**). From ~2585 to 1755 cal BP, PAR was ca. 0.2 mm a^{-1} and CAR less than 10 g C m^{-2} a^{-1}, suggesting the first phase of permafrost aggradation.

The next phase, from ~1600 to 800 cal BP (zone 2), was characterized by *S*. sect. *Cuspidata* and rapid peat and carbon accumulation (PAR of 1.1 mm a^{-1} and CAR of 45.4 g C m^{-2} a^{-1} (**Table 4**). First, the landscape likely opened after a wildfire ~1500 cal BP, and *P. mariana* temporarily disappeared. Poor-fen species *Warnstorfia fluitans* and *S. jensenii* aggr. increased, suggesting high water tables and possible permafrost thaw. *P. mariana* needles increased towards 800 cal BP, when vegetation again shifted from the dominance of *S*. sect. *Cuspidata* to hummock-level species *S. fuscum*. This shift marks the transition not only to drier conditions but also to slower peat accumulation (zone 3a between 800 and 50 cal BP). Around 755 cal BP, PAR dropped from 1.3 to 0.8 mm a^{-1} (**Figure 6**), suggesting a second phase of permafrost aggradation. A third reconstructed fire occurred approximately 730 cal BP (**Table 3**), but *Picea* trees did not totally disappear from the site, although the number of needle fragments decreased in peat. Zone 3b (~50 cal BP to the present) represents the contemporary vegetation of peat plateau bogs, dominated by *Rhododendron tomentosum* and *Cladonia* spp. lichens.

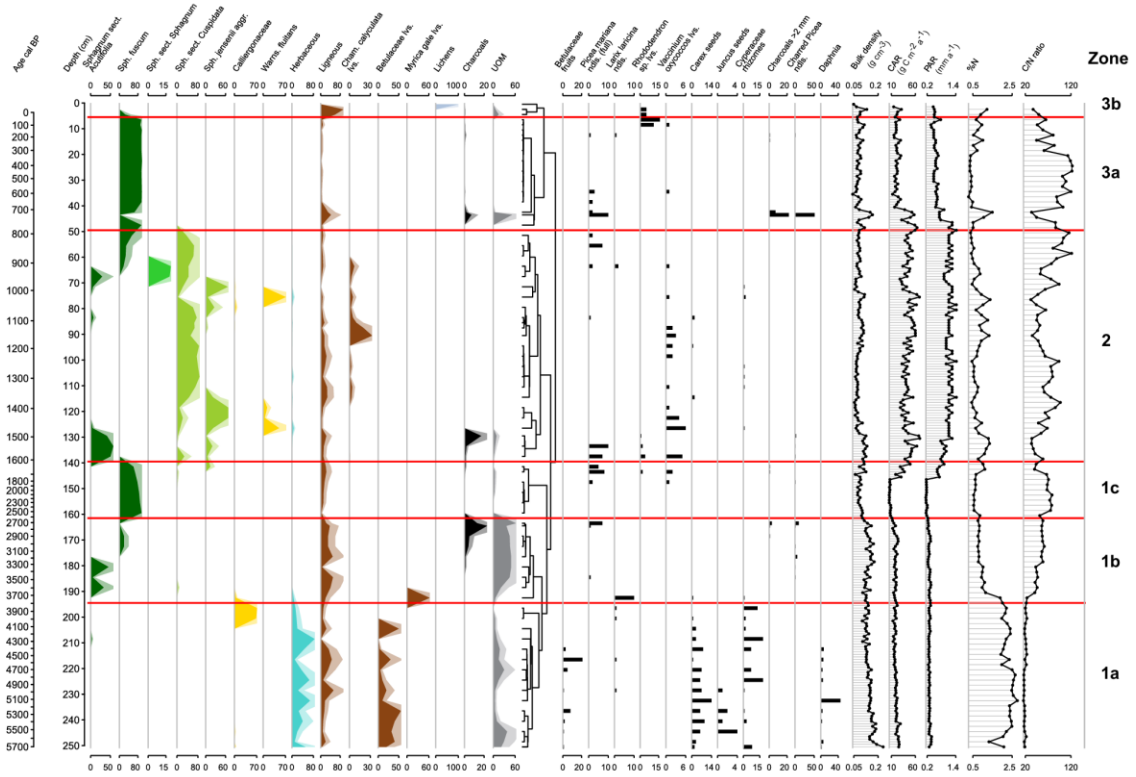

469

470 **Figure 6**. Treed peat plateau WAP27-1B. Plant macrofossil abundances (%) and counts, bulk density,
471 carbon (CAR) and peat (PAR) accumulation rates, and peat N content (%) and C/N ratio for WAP27-1B.
472 Different zones in the peat profile were identified using constrained hierarchical clustering (CONISS).

473

474 **4 Discussion**

475 **4.1 Peatland initiation and long-term carbon accumulation**

476 Since the retreat of the Laurentide Ice Sheet (LIS) and land emergence from the postglacial
477 Tyrell Sea, peatland initiation in the HBL has been primarily governed by the influence of
478 glacial isostatic adjustment (GIA) and climate (Dredge & Mott, 2003; Glaser et al., 2004;
479 Packalen et al., 2014). In WNP, peat thickness, age, and carbon mass increase from the coast
480 to inland (**Table 2; Supplemental Figure S11**). Peatland initiation dates to at least 6000 cal
481 BP in the boreal forest and extends into recent centuries along the coast, where new fens are
482 still formed following ongoing land emergence. These same gross patterns have been found
483 across the entire HBL complex (Dredge & Mott, 2003; Zhang et al., 2012; Packalen et al.,
484 2014, 2016; Li et al., 2025).

485 Among peatland types in WNP, total C masses and long-term C accumulation rates (LORCA)
486 were generally higher in treed/forested plateau bogs and polygonal peatlands than in non-

permafrost fens, reflecting the ongoing GIA and peatland succession from coastal fens to permafrost plateaus and polygons (Korhola et al., 1995). On average, plateau bogs store 71.7±21.4 (SE) kg C m^{-2}, polygonal peatlands 63.2±7.14 kg C m^{-2}, and non-permafrost fens 20.4±1.75 kg C m^{-2}. These values are lower than those generally found in the HBL complex, where a mean total C mass of 107 kg m^{-2} has been reported for bogs (incl. palsas and peat plateaus) and that of 81 kg m^{-2} for fens (Packalen et al., 2016). In addition to differences in growing season length and spatial variation in peat thickness (Packalen et al., 2016), lower C mass in WNP may be linked to permafrost aggradation and a subsequent decline in C accumulation (Camill et al., 2009; Lamarre et al., 2012; Robinson and Moore, 2000; Sannel and Kuhry, 2009). Most of these permafrost peatlands are currently covered by *Cladonia* spp. lichens that produce less biomass and decompose faster than *Sphagnum* mosses; therefore, limiting peat and C accumulation (Harris et al., 2018). Nevertheless, permafrost peatlands in WNP store a significant amount of soil carbon, some of which may be released to the atmosphere and exported to surface waters if the locally observed ice wedge degradation continues (Heffernan et al., 2024; Hugelius et al., 2020; Martin et al., 2017; Schuur et al., 2015, 2022; Treat et al., 2021; Wickham et al., 2020). The total carbon storage and C stocks across different peatland types in WNP are mapped and discussed in more detail in Cassidy et al. (*manuscript in prep*.).

4.2 Peatland development and permafrost dynamics across different vegetation zones

We focused on comparing peatland development and permafrost dynamics between low Arctic and subarctic tundra and northern boreal forests. Succession trajectories differed between vegetation zones. Most importantly, the treed bog phases that preceded polygons suggest that in the subarctic tundra, intermediate-centred polygons did not evolve from low-centred polygons, as is commonly interpreted (e.g., Mackay, 2000; Liljedahl et al., 2016; Vardy et al., 2005). Instead, our results suggest that ice-wedge polygons formed either in treed bogs or in open plateau bogs after trees disappeared between ~1330 and 780 cal BP (Payette et al., 1986). Furthermore, two main phases of permafrost aggradation were identified: the Dark Ages Cold Period (DACP; Helama et al., 2017) and the Little Ice Age (LIA; van Dijk et al., 2024), as suggested by sharp declines in peat accumulation (**Figure 7; Table 5**). DACP occurred ~1550–1185 cal BP (Helama et al., 2017), with extreme cold temperatures

~1430–1230 cal BP, a period named as the Late Antique Little Ice Age (LALIA; Büntgen et al., 2016; van Dijk et al., 2024). The LIA occurred approximately between 650 and 100 cal BP (1300–1850 CE), with evidence for a particularly cold period between 310 and 110 cal BP (1640–1840 CE; van Dijk et al., 2024). Correspondingly, a meta-analysis by Treat & Jones (2018) showed increased permafrost aggradation in many Canadian Arctic peatlands between 1500 and 750 cal BP.

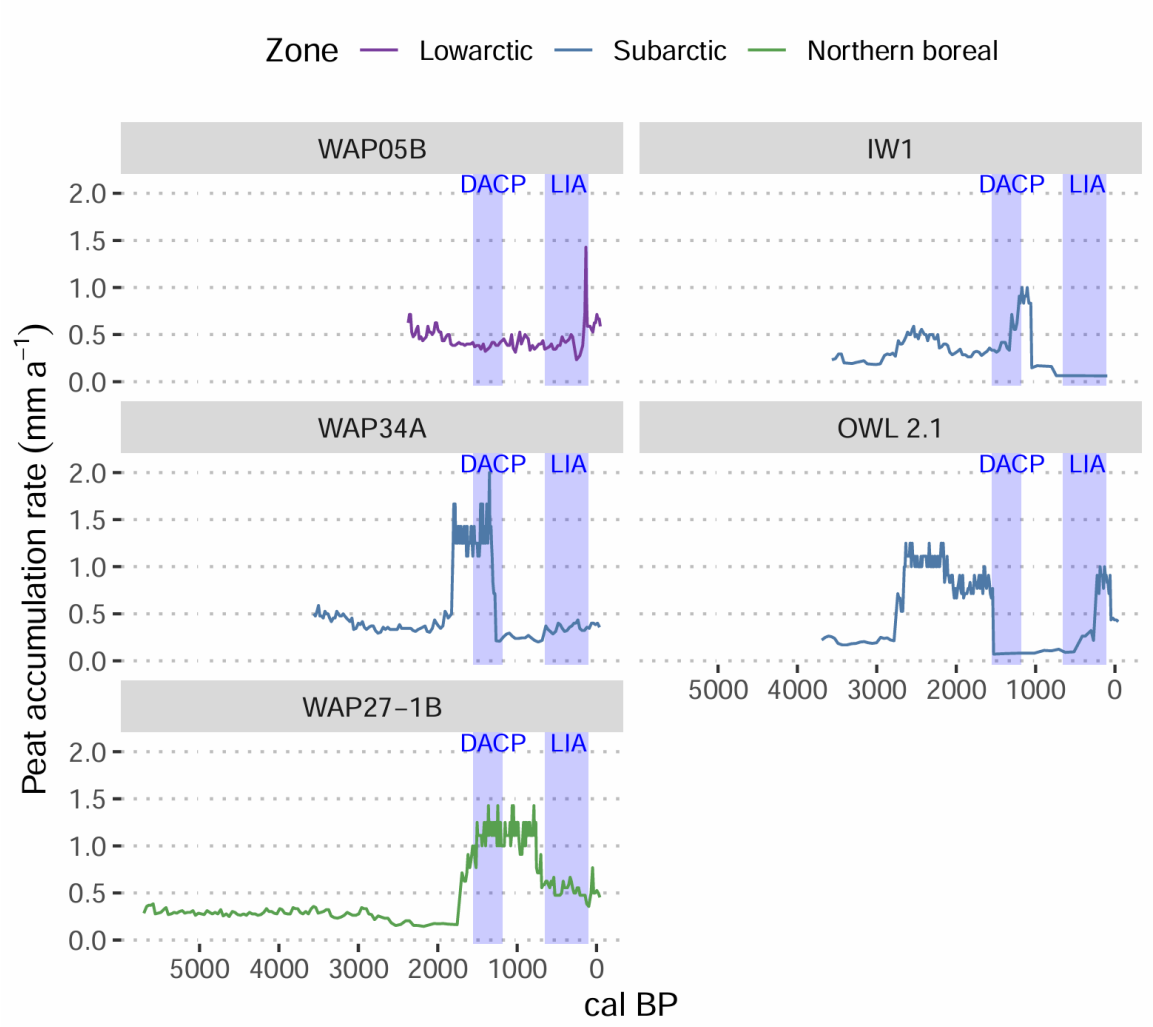

Figure 7. Peat accumulation rate (PAR; mm a-1) since peatland initiation. At the low Arctic site WAP05B, PAR has been relatively stable over time. At the subarctic polygons (IW1, WAP34A, and OWL 2.1), PAR declined rapidly around 1500–1050 cal BP, suggesting permafrost aggradation during the Dark Ages Cold Period (DACP; 1500–1185 cal BP, Helama et al., 2017). At the WAP27-1B peat plateau in the northern boreal forest, PAR was high through DACP and decreased around 700 cal BP, suggesting permafrost aggradation at the on set of the Little Ice Age (LIA).

4.2.1 Low Arctic tundra

In the low Arctic site WAP05B, peat began to accumulate ~2400 cal BP, and vegetation shifted from wet fen vegetation to the dominance of bog mosses (mostly *Dicranum* spp.) and dwarf shrubs ~200–175 cal BP, suggesting drying conditions with permafrost aggradation (Tarnocai & Zoltai, 1975; Vardy et al., 2005; Hichens-Bergström & Sannel, 2023) during the LIA. This timing of permafrost aggradation is supported by a decrease in peat N content (%) and an increase in C/N ratio (Treat et al., 2016). However, Treat et al. (2016) suggested that permafrost can also develop in tundra fens without a shift to bog vegetation, and the changes we observed in N% and C/N ratio at WAP05B are at least partly explained by the shift in vegetation type (Watmough et al., 2022). Alternatively, permafrost may have started to develop at WAP05B on newly exposed mineral soil or in coastal fens, as suggested by relatively stable N% and C/N ratios before the shift to bog vegetation ~200 cal BP (Shur & Jorgenson, 2007; Sannel & Kuhry, 2009).

At WAP05B, intermediate-centred polygons might have developed from low-centred polygons ~200 cal BP. The present-day polygon was preceded by wet fen vegetation with Calliergonaceae mosses and sedges, commonly found in low-centred polygons (De Klerk et al., 2011; Mackay, 2000; Wolter et al., 2016). Multiple Chironomidae head capsules and *Daphnia* spp. resting eggs were also found in this peat layer, which dates from ~1100 to 200 cal BP (**Figure 2**), suggesting an aquatic habitat. At the nearby subarctic site (IW1), permafrost likely developed ~1050 cal BP, supporting permafrost aggradation and polygon formation before the LIA at WAP05B. Ouzilleau Samson et al. (2010) also reported a shift to colder conditions ~1100 cal BP, inferred from paleoecological records from permafrost peatlands on the eastern coast of Hudson Bay in subarctic Quebec. If permafrost developed at our site around this time, ice wedge degradation could explain the formation of a dry polygon ~200–175 cal BP. Moreover, the timing of the fen-bog transition is somewhat uncertain because the past few centuries are difficult to date accurately using ^{14}C. Therefore, it is possible that the dry polygon formed due to permafrost thaw slightly later, during the warming after the LIA.

At present, small and shallow ponds are common in WNP, but we have not found any low-centred polygons. Thus, we conclude that permafrost likely developed in the low Arctic tundra during the DACP and dry polygons formed at the end of LIA, but the exact successional

pathway remains uncertain. Previous studies have reported accelerated formation of high-centred polygons over the past ~30 years or the recent century (Abolt et al., 2020; Wolter et al., 2018), that indicates the low Arctic tundra in WNP may see an increase of high-centred polygons in the coming decades.

4.2.2 Subarctic tundra

At subarctic polygonal peatlands in WNP, peat generally started to accumulate on recently exposed mineral soil between 3700 and 3200 cal BP. Paleoreconstructions suggest that the shift from fen to *Sphagnum* bog vegetation occurred ~2850–2350 cal BP. This shift was followed by a treed bog phase, mainly with *Sphagnum fuscum* and *Picea mariana* (and some *P. glauca*). At the WAP34A site, an open *S. fuscum* bog preceded the treed bog phase, and at OWL 2.1, vegetation shifted from the dominance of *S. fuscum type* to that of *S. sect. Cuspidata* ~2200 cal BP. Similarly, a previous study conducted in the region, but in treed plateau bogs, concluded that the vegetation in the area has been characterized by *S. fuscum*, *P. marina*, and *P. glauca* for the past six millennia (Dredge & Mott, 2003). In the subarctic tundra, however, spruce disappeared from the present-day polygonal peatlands between ~1330 and 780 cal BP, depending on the site, which were not recorded in the Dredge and Mott (2003) pollen diagrams from the treed plateau bogs.

Permafrost aggradation likely began in the subarctic WNP during the cold conditions of DACP (Helama et al., 2017), as indicated by reduced peat and carbon accumulation starting between 1500 and 1050 cal BP. The sharp declines in PAR and CAR, observed at all three sites (**Figure 7**), likely reflect drying and increased decomposition in the surface peat, which often follow permafrost aggradation (Camill et al., 2009; Lamarre et al., 2012; Robinson and Moore, 2000; Sannel and Kuhry, 2009). It is noteworthy that the rapid decrease in PAR and CAR did not coincide with a shift from fen to *Sphagnum* bog vegetation, which has been used as a proxy for permafrost aggradation (e.g., Tarnocai & Zoltai, 1975; Vardy et al., 2005; Hichens-Bergström & Sannel, 2023). Instead, permafrost likely developed in response to a shift toward colder climatic conditions and peat accumulation (Shur & Jorgenson, 2007). Peat N content (%) decreased, and the C/N ratio increased with the shift from fen to bog vegetation, in line with previous meta-analyses (Loisel et al., 2014; Treat et al., 2016; Watmough et al., 2022).

Thus, both N content (%) and C/N ratios mainly reflected vegetation type. At OWL 2.1, however, the lowest %N values were found in surface peat (21-22 cm) with ligneous plant remains, possibly indicating drier conditions and a second phase of permafrost aggradation ~210 cal BP (Treat et al., 2016), after a short thaw phase approximately between ~890–520 cal BP.

Spruce (*P. mariana* and *P. glauca*) did not disappear synchronously with the interpreted permafrost aggradation, but it is also likely linked to shifts toward colder climatic conditions during the DACP and later during the onset of LIA (Helama et al., 2017; Delwaide et al., 2021; van Dijk et al., 2024). At WAP34A and OWL 2.1, spruce disappeared approximately 500–600 years after permafrost aggradation, ~780–890 cal BP. At IW1, spruces disappeared already ~1330 cal BP during DACP, while permafrost aggradation likely occurred ~1050 cal BP. Reduced growth of *Picea mariana* during DACP and at the onset of LIA has been evidenced by pollen data from marine sediments from eastern Hudson Bay (Vallerand et al., 2024) and tree-ring data from subarctic Quebec, northeastern Canada (Vallée & Payette, 2004; Arseneault et al., 2013; Gennaretti et al., 2014). Local wildfires and permafrost thaw at the end of the Medieval Warm Period (MWP; maximum temperatures ~970–770 cal BP; van Dijk et al., 2024) may have also contributed to the disappearance of trees (Camill et al., 2009). Charcoals were found in the OWL 2.1 core at a depth of 31–26 cm, while the last (the most recent) *Picea* needles were observed at 31–30 cm. Based on the age-depth model, at least one wildfire occurred roughly between 900 and 500 cal BP, overlapping with the end of MWP and early LIA (van Dijk et al., 2024). Following this, *Warnstorfia fluitans* (aggregate) and wet-habitat species of *Sphagnum* sect. *Cuspidata* increased, likely indicating permafrost thaw (Arlen-Pouliot & Bhiry, 2005; Erlington et al., 2024; Kuhry, 2008; Robinson & Moore, 2000). Permafrost thaw may have also caused trees to die (Dearborn et al., 2020) during the short thaw phase, roughly ~890–520 cal BP.

The disappearance of trees may also be connected to the formation of polygonal ice wedges, but it is difficult to determine which one occurred first. On the one hand, ice-wedge polygons may form in subarctic peatlands after trees disappear, enabling deep frost cracking (Payette et al, 1986). On the other hand, the formation of polygonal ice wedges and subsequent drainage may have hampered tree growth (Ovenden, 1982), which could explain why spruces disappeared after the interpreted permafrost aggradation at two out of three subarctic sites.

624 The detailed evolution of ice wedges is outside the scope of our study, but we collected and
625 dated one peat profile (WAP34B) from an ice-wedge trough. Peat started to accumulate on
626 top of the ice wedge ~570 cal BP, and correspondingly, *S. lenense* replaced *S. fuscum* in the
627 polygon centre at WAP34A between 600 and 500 cal BP. Both are hummock-forming species,
628 and their distribution areas partly overlap, but *S. fuscum* is a more generalist bog species
629 than *S. lenense*, which predominantly grows in arctic tundra, including dry polygon centres
630 (Ovenden, 1982). A similar shift toward *S. lenense* dominance and later toward lichen
631 dominance was also observed at the OWL 2.1 site during the LIA. Our results suggest that
632 polygonal ice-wedges formed at the onset of the LIA. In fact, Kasper & Allard (2001) reported
633 intense ice-wedge activity during the LIA on the eastern coast of Hudson Bay, but further
634 research is needed on ice-wedge evolution and activity in the northwestern HBL.

635

636 *4.2.3 Northern boreal forest*

637 The development history of our treed plateau site (WAP27-1B) roughly follows the same
638 patterns documented by Kuhry (2008) in a treed plateau approximately 20 km northwest
639 along the Hudson Bay railroad. At WAP27-1B, peat accumulation began ~5700 cal BP, and the
640 fen-bog transition occurred ~3700 cal BP. Kuhry (2008) estimated that the first phase of
641 permafrost aggradation may have occurred ~2250 cal BP. At WAP27-1B, low PAR and CAR
642 values suggest the first phase of permafrost aggradation ~2585–1755 cal BP (Camill et al.,
643 2009; Lamarre et al., 2012; Robinson & Moore, 2000). A wildfire occurred in the area ~2750
644 cal BP, which, on the one hand, may have burned the insulating peat and vegetation,
645 triggering permafrost aggradation (Shur & Jorgenson, 2007). On the other hand, the loss of
646 peat during the wildfire and diminished peat accumulation in response to fire could explain
647 the low PAR and CAR values (Kuhry, 1994; Robinson & Moore, 2000; Sannel & Kuhry, 2009). In
648 either case and in contrast to our subarctic sites, northern boreal peatlands may have
649 remained permafrost-free at least from 1600 to 700 cal BP, throughout the DACP and until the
650 onset of the LIA. This was indicated by relatively high PAR and CAR values and the abundance
651 of wet-habitat moss species, including *Sphagnum jensenii* (aggregate) and *Warnstorfia*
652 *fluitans*. PAR and CAR diminished ~755 cal BP, suggesting permafrost aggradation at the
653 onset of LIA (Camill et al., 2009; Lamarre et al., 2012; Robinson and Moore, 2000; Sannel and
654 Kuhry, 2009). Correspondingly, Kuhry (2008) concluded that in northern boreal forests of

655 northern Manitoba, treed plateau bogs formed ~800–400 cal BP, or alternatively, permafrost
656 developed earlier under wet conditions.

657

658 **Conclusions**

659 Paleoreconstructions from the northernmost peatlands in HBL suggest relatively recent
660 permafrost aggradation in the region. The sharp decline in peat and carbon accumulation
661 during cold periods best indicated the timing of permafrost aggradation. In the low Arctic and
662 subarctic tundra, permafrost likely developed ~1500–1050 cal BP during the DACP. Since its
663 aggradation, permafrost appeared relatively stable across the subarctic tundra, except for
664 one short thaw phase following a wildfire at the OWL 2.1 site. In the northern boreal forest,
665 the lowest peat accumulation rates were observed ~2585–1755 cal BP, which may relate to a
666 wildfire, permafrost aggradation, or both. Peat and C accumulation rates again decreased
667 ~755 cal BP at the onset of the LIA, indicating permafrost aggradation. Due to its relatively
668 recent origin, permafrost in the northwestern HBL may be particularly vulnerable to thaw
669 under present warming.

670 Our paleoecological reconstructions further suggest that in subarctic polygonal peatlands,
671 permafrost aggradation occurred in response to shifts to colder climatic conditions and the
672 accumulation of *Sphagnum* peat, but it did not coincide with fen-bog transitions. In the
673 subarctic, dry intermediate-centred polygons did not evolve from wet, low-centred polygons,
674 as commonly interpreted. Instead, the shift from treed bog vegetation with *Picea mariana*
675 and *P. glauca*, first to open bog vegetation, and finally to lichen-dominated polygons,
676 suggests that ice-wedge polygons formed in *Sphagnum*-dominated peat plateaus, following
677 the disappearance of trees between ~1330 and 780 cal BP. The disappearance of trees was
678 likely linked to a shift to colder climatic conditions and shorter growing seasons during DACP
679 and at the onset of LIA, although local wildfires at the end of the MWP may have contributed
680 to the opening of the canopy. In the low Arctic tundra, however, the study site was
681 characterized by fen vegetation until the end of the LIA, when dry polygons developed, but
682 the exact successional pathway remains uncertain. Considering these historical differences
683 would be critical in future studies, as ultimately, the degree of decomposition and type of

permafrost peat (fen vs. bog), underlying the lichen-dominated polygons, affects the climate-carbon feedbacks in a warming climate.

CRediT author statement

All authors contributed substantially to data collection and reviewed and approved the final version of the manuscript. The authors also contributed to the following tasks: Conceptualization (THMK, MG, LG, FB), Methodology (THMK, MG, NKS, LG), Writing – original draft (THMK), Writing – review and editing (MG, LG, JA, MB, FB, LAF, NKS, AEC, AC, LCW, SF), Visualization (THMK, AC), Supervision (MG, NKS), Project administration (MG, AEC, KR), Funding acquisition (MG, KR, LG, FB).

Declaration of competing interest

The authors declare that they have no competing interests.

Acknowledgments

This work was supported by funding from Parks Canada and ANR grant (Arctic-Peat, no. ANR 2020 – CE01-001) to LG. The work of FB, JA, and LCW was supported by NSERC Discovery and Northern Research Supplement funding, Polar Continental Shelf Program (PCSP), and Northern Research Fund (NRF) from Churchill Northern Studies Centre (CNSC). We thank the Parks Canada field unit staff in Churchill for support during field campaigns, especially Erica Gillis, Nicole Rogowsky, Jesse Shirton, and Russell Turner. We thank Seal River Guardians Calvin Clipping, Sadie Dumas, and Augustine Tessessage for their assistance in collecting peat cores. We are grateful to Joëlle Cormier, Gauthier Genez, Raphaëlle Grégoire, and Guillaume Provost for their assistance in laboratory work. We also appreciate the support of Léonie Perrier during this project. We acknowledge the PAPC platform at the CRBE laboratory (France) and the light stable isotope geochemistry laboratory at Geotop-UQAM (Canada) for C and N analysis. Fieldwork in the Churchill Wildlife Management Area was conducted under permits 78303365 (2024) and 90026228 (2025) from Manitoba Conservation.

References

Abolt, C. J., Young, M. H., Atchley, A. L., Harp, D. R., & Coon, E. T. (2020). Feedbacks between surface deformation and permafrost degradation in ice wedge polygons, Arctic Coastal Plain, Alaska. *Journal of Geophysical Research: Earth Surface, 125*(3), e2019JF005349. https://doi.org/10.1029/2019JF005349

Arlen-Pouliot, Y., & Bhiry, N. (2005). Palaeoecology of a palsa and a filled thermokarst pond in a permafrost peatland, subarctic Québec, Canada. *The Holocene, 15*(3), 408-419. https://doi.org/10.1191/0959683605hl818r

Ayoutte, G. & Rochefort, L. (2019). Les sphaignes de l'Est du Canada – Clé d'identification visuelle et cartes de répartition. Les Éditions JFD Inc., Montréal, Québec, Canada. ISBN: 978-2-924651-99-5

Baldwin, K., Allen, L., Basquill, S., Chapman, K., Downing, D., Flynn, N., MacKenzie, W., Major, M., Meades, W., Meidinger, D., Morneau, C., Saucier, J-P., Thorpe, J., Uhlig, P. (2019). Vegetation Zones of Canada: a Biogeoclimatic Perspective. [Map] Scale 1:5,000,000. *Natural Resources Canada, Canadian Forest Service. Great Lake Forestry Center, Sault Ste. Marie, ON, Canada*.

Biskaborn, B. K., Smith, S. L., Noetzli, J, Matthes, H., Vieira, G., Streletskiy, D. A., ... & Lantuit, H. (2019). Permafrost is warming at a global scale. *Nature communications*, *10*(1), 264. https://doi.org/10.1038/s41467-018-08240-4

Blaauw, M. & Christen, J.A. (2011). Flexible paleoclimate age-depth models using an autoregressive gamma process. *Bayesian Analysis, 6*(3), 457-474. https://doi.org/10.1214/11-BA618

Bouchard, F., Turner, K. W., MacDonald, L. A., Deakin, C., White, H., Farquharson, N., ... & Edwards, T. W. D. (2013). Vulnerability of shallow subarctic lakes to evaporate and desiccate when snowmelt runoff is low. *Geophysical Research Letters, 40*(23), 6112-6117. https://doi.org/10.1002/2013GL058635

Büntgen, U., Myglan, V. S., Ljungqvist, F. C., McCormick, M., Di Cosmo, N., Sigl, M., Jungclaus. J., Wagner, S., Krusic, P. J., Esper, J., Kaplan, J. O., de Vaan, M. A., C., Luterbacher, J., Wacker, L., Tegel, W., & Kirdyanov, A. V. (2016). Cooling and societal change during the Late Antique Little Ice Age from 536 to around 660 AD. *Nature Geoscience*, *9*(3), 231-236. https://doi.org/10.1038/ngeo2652

Camill, P., Barry, A., Williams, E., Andreassi, C., Limmer, J., & Solick, D. (2009). Climate-vegetation-fire interactions and their impact on long-term carbon dynamics in a boreal peatland landscape in northern Manitoba, Canada. *Journal of Geophysical Research: Biogeosciences, 114*(G4). https://doi.org/10.1029/2009JG001071

Cassidy A. E., Kolari, T. H. M., Collingwood, A., Richardson, K., ..., & Garneau, M. Mapping carbon stocks across peatlands in Wapusk National Park. (*manuscript in prep.*)

Chambers, F. M., Beilman, D. W., & Yu, Z. (2011). Methods for determining peat humification and for quantifying peat bulk density, organic matter and carbon content for palaeostudies of climate and peatland carbon dynamics. *Mires and peat, 7,* 07.

Dalton, A. S., Dulfer, H. E., Margold, M., Heyman, J., Clague, J. J., Froese, D. G., Gauthier, M. S., Hughes, A. L. C., Jennings, C. E., Norris, S. L., & Stoker, B. J. (2023). Deglaciation of the north American ice sheet complex in calendar years based on a comprehensive database of chronological data: NADI-1. *Quaternary Science Reviews, 321*, 108345. https://doi.org/10.1016/j.quascirev.2023.108345

De Klerk, P., Donner, N., Karpov, N. S., Minke, M., & Joosten, H. (2011). Short-term dynamics of a low-centred ice-wedge polygon near Chokurdakh (NE Yakutia, NE Siberia) and climate change during the last ca 1250 years. *Quaternary Science Reviews, 30*(21-22), 3013-3031. https://doi.org/10.1016/j.quascirev.2011.06.016

Dearborn, K. D., Wallace, C. A., Patankar, R., & Baltzer, J. L. (2021). Permafrost thaw in boreal peatlands is rapidly altering forest community composition. *Journal of Ecology*, *109*(3), 1452-1467. https://doi.org/10.1111/1365-2745.13569

Delwaide, A., Asselin, H., Arseneault, D., Lavoie, C., & Payette, S. (2021). A 2233-year tree-ring chronology of subarctic black spruce (Picea mariana): growth forms response to long-term climate change. *Ecoscience, 28*(3-4), 399-419. https://doi.org/10.1080/11956860.2021.1952014

Dredge, L. A., & Mott, R. J. (2003). Holocene pollen records and peatland development, northeastern Manitoba. *Géographie physique et Quaternaire, 57*(1), 7-19. https://doi.org/10.7202/010328ar

Ellis, C. J., Rochefort, L., Gauthier, G., & Pienitz, R. (2008). Paleoecological evidence for transitions between contrasting landforms in a polygon-patterned High Arctic wetland. *Arctic, Antarctic, and Alpine Research, 40*(4), 624-637. https://doi.org/10.1657/1523-0430(07-059)[ELLIS]2.0.CO;2

Errington, R. C., Macdonald, S. E., & Bhatti, J. S. (2024). Rate of permafrost thaw and associated plant community dynamics in peatlands of northwestern Canada. *Journal of Ecology, 112*(7), 1565-1582. https://doi.org/10.1111/1365-2745.14339

Faubert, J. (2014). Flore des bryophytes du Québec-Labrador. Volume 3 : Mousses, seconde partie. Société québécoise bryologie, Saint-Valérien, Québec, Canada. 456 p. ISBN : 978-2-9813260-2-7

Fortier, D., & Allard, M. (2005). Frost-cracking conditions, Bylot Island, eastern Canadian Arctic archipelago. *Permafrost and Periglacial Processes, 16*(2), 145-161. https://doi.org/10.1002/ppp.504

French, H., & Shur, Y. (2010). The principles of cryostratigraphy. *Earth-Science Reviews, 101*(3-4), 190-206. https://doi.org/10.1016/j.earscirev.2010.04.002

Fritz, M., Wolter, J., Rudaya, N., Palagushkina, O., Nazarova, L., Obu, J., ... & Wetterich, S. (2016). Holocene ice-wedge polygon development in northern Yukon permafrost peatlands (Canada). *Quaternary Science Reviews, 147*, 279-297. https://doi.org/10.1016/j.quascirev.2016.02.008

Gauthier, M. S., Kelley, S. E., & Hodder, T. J. (2020). Lake Agassiz drainage bracketed Holocene Hudson Bay ice saddle collapse. *Earth and Planetary Science Letters, 544,* 116372. https://doi.org/10.1016/j.epsl.2020.116372

Gennaretti, F., Arseneault, D., Nicault, A., Perreault, L., & Bégin, Y. (2014). Volcano-induced regime shifts in millennial tree-ring chronologies from northeastern North America. *Proceedings of the National Academy of Sciences*, *111*(28), 10077-10082. https://doi.org/10.1073/pnas.1324220111

Glaser, P. H., Hansen, B. C., Siegel, D. I., Reeve, A. S., & Morin, P. J. (2004). Rates, pathways and drivers for peatland development in the Hudson Bay Lowlands, northern Ontario, Canada. *Journal of Ecology, 92*(6), 1036-1053. https://doi.org/10.1111/j.0022-0477.2004.00931.x

Harris, L. I., Moore, T. R., Roulet, N. T., & Pinsonneault, A. J. (2018). Lichens: A limit to peat growth? *Journal of Ecology, 106*(6), 2301-2319. https://doi.org/10.1111/1365-2745.12975

Heffernan, L., Kothawala, D. N., & Tranvik, L. J. (2024). Terrestrial dissolved organic carbon in northern permafrost. *The Cryosphere, 18*(3), 1443-1465. https://doi.org/10.5194/tc-18-1443-2024

Helama, S., Jones, P. D., & Briffa, K. R. (2017). Dark Ages Cold Period: A literature review and directions for future research. *The Holocene, 27*(10), 1600-1606. https://doi.org/10.1177/0959683617693898

Hichens-Bergström, M., & Sannel, A. B. K. (2023). Permafrost development in northern Fennoscandian peatlands since the mid-Holocene. *Arctic, Antarctic, and Alpine Research*, *55*(1), 2250035. https://doi.org/10.1080/15230430.2023.2250035

Hugelius, G., Loisel, J., Chadburn, S., Jackson, R. B., Jones, M., MacDonald, G., Marushchak, M., Olefeldt, D., Packalen, M., Siewert, M. B., Treat, C., Turetsky, M., Voigt, C., & Yu, Z. (2020). Large stocks of peatland carbon and nitrogen are vulnerable to permafrost thaw. *Proceedings of the National Academy of Sciences, 117*(34), 20438-20446. https://doi.org/10.1073/pnas.1916387117

Jones, M. C., Grosse, G., Treat, C., Turetsky, M., Anthony, K. W., & Brosius, L. (2023). Past permafrost dynamics can inform future permafrost carbon-climate feedbacks. *Communications Earth & Environment, 4*(1), 272. https://doi.org/10.1038/s43247-023-00886-3

Jorgenson, M. T., Kanevskiy, M. Z., Jorgenson, J. C., Liljedahl, A., Shur, Y., Epstein, H., Kent, K., Griffin, C. G., Daanen, R., Boldenow, M., Orndal, K., Witharana, C., & Jones, B. M. (2022). Rapid transformation of tundra ecosystems from ice-wedge degradation. *Global and Planetary Change, 216*, 103921. https://doi.org/10.1016/j.gloplacha.2022.103921

Jorgenson, M. T., Shur, Y. L., & Pullman, E. R. (2006). Abrupt increase in permafrost degradation in Arctic Alaska. *Geophysical Research Letters, 33*(2). https://doi.org/10.1029/2005GL024960

Juggins, S. (2024) rioja: Analysis of Quaternary Science Data, R package version (1.0-7). https://cran.r-project.org/package=rioja

Juggins, S. (2025) riojaPlot: Stratigraphic diagrams in R, package version (0.1-24). https://github.com/nsj3/riojaPlot

Kanevskiy, M., Shur, Y., Jorgenson, T., Brown, D. R., Moskalenko, N., Brown, J., Walker, D. A., Raynolds, M. K., & Buchhorn, M. (2017). Degradation and stabilization of ice wedges: Implications for assessing risk of thermokarst in northern Alaska. *Geomorphology, 297*, 20-42. https://doi.org/10.1016/j.geomorph.2017.09.001

Kasper, J. N., & Allard, M. (2001). Late-Holocene climatic changes as detected by the growth and decay of ice wedges on the southern shore of Hudson Strait, northern Québec, Canada. *The Holocene, 11*(5), 563-577. https://doi.org/10.1191/095968301680223512

Kirkwood, J. A. H., Roy-Léveillée, P., Mykytczuk, N., Packalen, M., McLaughlin, J., Laframboise, A., & Basiliko, N. (2021). Soil microbial community response to permafrost degradation in palsa fields of the Hudson Bay Lowlands: Implications for greenhouse gas production in a warming climate. *Global Biogeochemical Cycles, 35*(6), e2021GB006954. https://doi.org/10.1029/2021GB006954

Kokelj, S. V., Lantz, T. C., Wolfe, S. A., Kanigan, J. C., Morse, P. D., Coutts, R., ... & Burn, C. R. (2014). Distribution and activity of ice wedges across the forest-tundra transition, western Arctic Canada. *Journal of Geophysical Research: Earth Surface, 119*(9), 2032-2047. https://doi.org/10.1002/2014JF003085

Korhola, A., Tolonen, K., Turunen, J., & Jungner, H. (1995). Estimating long-term carbon accumulation rates in boreal peatlands by radiocarbon dating. *Radiocarbon, 37*(2), 575-584. https://doi.org/10.1017/S0033822200031064

Kuhry, P. (1994). The role of fire in the development of *Sphagnum*-dominated peatlands in western boreal Canada. *Journal of Ecology*, 899-910.

Kuhry, P. (2008). Palsa and peat plateau development in the Hudson Bay Lowlands, Canada: timing, pathways and causes. *Boreas, 37*(2), 316-327. https://doi.org/10.1111/j.1502-3885.2007.00022.x

Laine, J., Harju, P., Timonen, T., Laine, A., Tuittila, E.-S., Minkkinen, K., & Vasander, H. (2009). The Intricate Beauty of Sphagnum Mosses – A Finnish Guide to Identification. University of Helsinki Department of Forest Ecology Publications, *39,* 1-190. ISBN: 978-952-10-5617-8

Lamarre, A., Garneau, M., & Asnong, H. (2012). Holocene paleohydrological reconstruction and carbon accumulation of a permafrost peatland using testate amoeba and macrofossil analyses, Kuujjuarapik, subarctic Québec, Canada. *Review of Palaeobotany and Palynology, 186,* 131-141. https://doi.org/10.1016/j.revpalbo.2012.04.009

Langer, M., Nitzbon, J., Groenke, B., Assmann, L. M., Schneider von Deimling, T., Stuenzi, S. M., & Westermann, S. (2024). The evolution of Arctic permafrost over the last 3 centuries from ensemble simulations with the CryoGridLite permafrost model. *The Cryosphere, 18*(1), 363-385. https://doi.org/10.5194/tc-18-363-2024

Li, Y., Han, D., Rogers, C. A., Finkelstein, S. A., Hararuk, O., Waddington, J. M., Barreto, C., McLaughlin, J. W., Snider, J., & Gonsamo, A. (2025). Peat depth and carbon storage of the Hudson Bay Lowlands, Canada. *Geophysical Research Letters, 52*(2), e2024GL110679. https://doi.org/10.1029/2024GL110679

Liljedahl, A. K., Boike, J., Daanen, R. P., Fedorov, A. N., Frost, G. V., Grosse, G., Hinzman, L. D., Iijma, Y., Jorgenson, J. C., Matveyeva, N., Necsoiu, M., Raynolds, M. K., Romanovsky, V. E., Schulla, J., Tape, K. D., Walker, D. A., Wilson, C. J., Yabuki, H., & Zona, D. (2016). Pan-Arctic ice-wedge degradation in warming permafrost and its influence on tundra hydrology. *Nature Geoscience, 9*(4), 312-318. https://doi.org/10.1038/ngeo2674

Loisel, J., Yu, Z., Beilman, D. W., Camill, P., Alm, J., Amesbury, M. J., ... & Zhou, W. (2014). A database and synthesis of northern peatland soil properties and Holocene carbon and nitrogen accumulation. *The Holocene, 24*(9), 1028-1042. https://doi.org/10.1177/0959683614538073

Mackay, J. R. (1993). Air temperature, snow cover, creep of frozen ground, and the time of ice-wedge cracking, western Arctic coast. *Canadian Journal of Earth Sciences, 30*(8), 1720-1729. https://doi.org/10.1139/e93-151

MacKay, J. R. (2000). Thermally induced movements in ice-wedge polygons, western Arctic coast: a long-term study. *Géographie physique et Quaternaire, 54*(1), 41-68. https://doi.org/10.7202/004846ar

Martin, A. F., Lantz, T. C., & Humphreys, E. R. (2017). Ice wedge degradation and CO2 and CH4 emissions in the Tuktoyaktuk Coastlands, Northwest Territories. *Arctic Science, 4*(1), 130-145. https://doi.org/10.1139/as-2016-0011

Mauquoy, D., Hughes, P. D. M., & Van Geel, B. (2010). A protocol for plant macrofossil analysis of peat deposits. *Mires and Peat, 7,* 06.

Millard, A. R. (2014). Conventions for reporting radiocarbon determinations. *Radiocarbon, 56*(2), 555-559. https://doi.org/10.2458/56.17455

Obu, J., Westermann, S., Bartsch, A., Berdnikov, N., Christiansen, H. H., Dashtseren, A., ... & Zou, D. (2019). Northern Hemisphere permafrost map based on TTOP modelling for 2000–2016 at 1 km^2 scale. *Earth-Science Reviews, 193*, 299-316. https://doi.org/10.1016/j.earscirev.2019.04.023

Ouzilleau Samson, D., Bhiry, N., & Lavoie, M. (2010). Late-Holocene palaeoecology of a polygonal peatland on the south shore of Hudson Strait, northern Québec, Canada. *The Holocene, 20*(4), 525-536. https://doi.org/10.1177/095968360935658

Ovenden, L. (1982). Vegetation history of a polygonal peatland, northern Yukon. *Boreas, 11*(3), 209-224. https://doi.org/10.1111/j.1502-3885.1982.tb00715.x

Packalen, M. S., Finkelstein, S. A., & McLaughlin, J. W. (2014). Carbon storage and potential methane production in the Hudson Bay Lowlands since mid-Holocene peat initiation. *Nature communications, 5*(1), 4078. https://doi.org/10.1038/ncomms5078

Packalen, M. S., Finkelstein, S. A., & McLaughlin, J. W. (2016). Climate and peat type in relation to spatial variation of the peatland carbon mass in the Hudson Bay Lowlands, Canada. *Journal of Geophysical Research: Biogeosciences, 121*(4), 1104-1117. https://doi.org/10.1002/2015JG002938

Parmentier, F. J. W., Nilsen, L., Tømmervik, H., Meisel, O. H., Bröder, L., Vonk, J. E., Westermann, S., Semenchuk, P. R., & Cooper, E. J. (2024). Rapid ice-wedge collapse and permafrost carbon loss triggered by increased snow depth and surface runoff. *Geophysical Research Letters, 51*(11), e2023GL108020. https://doi.org/10.1029/2023GL108020

Payette, S., Gauthier, L. & Grenier, I. (1986). Dating ice-wedge growth in subarctic peatlands following deforestation. *Nature, 322*, 724–727. https://doi.org/10.1038/322724a0

Ponomarenko, S., Quirouette, J., Sharma, R. and D. McLennan. (2014). Ecotype Mapping Report for Wapusk National Park. Monitoring and Ecological Information. *Natural Resource Conservation*. *Parks Canada*. *Gatineau, QC, Canada*.

Ramsey, C. B. (2009). Bayesian analysis of radiocarbon dates. *Radiocarbon, 51*(1), 337-360. https://doi.org/10.1017/S0033822200033865

Rantanen, M., Karpechko, A. Y., Lipponen, A., Nordling, K., Hyvärinen, O., Ruosteenoja, K., Vihma, T., & Laaksonen, A. (2022). The Arctic has warmed nearly four times faster than the globe since 1979. *Communications earth & environment, 3*(1), 168. https://doi.org/10.1038/s43247-022-00498-3

R Core Team (2025). R: A Language and Environment for Statistical Computing. R Foundation for Statistical Computing, Vienna, Austria. https://www.R-project.org

Reimer, P. J., Austin, W. E., Bard, E., Bayliss, A., Blackwell, P. G., Ramsey, C. B., ... & Talamo, S. (2020). The IntCal20 Northern Hemisphere radiocarbon age calibration curve (0–55 cal kBP). *Radiocarbon, 62*(4), 725-757. https://doi.org/10.1017/RDC.2020.41

Robinson, S. D., & Moore, T. R. (2000). The influence of permafrost and fire upon carbon accumulation in high boreal peatlands, Northwest Territories, Canada. *Arctic, Antarctic, and Alpine Research, 32*(2), 155-166. https://doi.org/10.1080/15230430.2000.12003351

Sannel, A. B. K., & Kuhry, P. (2008). Long-term stability of permafrost in subarctic peat plateaus, west-central Canada. *The Holocene, 18*(4), 589-601. https://doi.org/10.1177/0959683608089658

Sannel, A. B. K., & Kuhry, P. (2009). Holocene peat growth and decay dynamics in sub-arctic peat plateaus, west-central Canada. *Boreas, 38*(1), 13-24. https://doi.org/10.1111/j.1502-3885.2008.00048.x

Sella, G. F., Stein, S., Dixon, T. H., Craymer, M., James, T. S., Mazzotti, S., & Dokka, R. K. (2007). Observation of glacial isostatic adjustment in “stable” North America with GPS. *Geophysical Research Letters, 34*(2). https://doi.org/10.1029/2006GL027081

Schirrmeister, L., Bobrov, A., Raschke, E., Herzschuh, U., Strauss, J., Pestryakova, L. A., & Wetterich, S. (2018). Late Holocene ice-wedge polygon dynamics in northeastern Siberian coastal lowlands. *Arctic, Antarctic, and Alpine Research, 50*(1), e1462595. https://doi.org/10.1080/15230430.2018.1462595

Schulze, C., Sonnentag, O., Emmerton, C. A., Harris, L., Alcock, H., Marouelli, K., Hould Gosselin, G., Knox, S. H., Howard, R., Skeeter, J., Moore, P., Nesic, Z., & Olefeldt, D. (2025). Large carbon losses from burned permafrost peatlands during post-fire succession. *Geophysical Research Letters, 52*(19), e2025GL118344. https://doi.org/10.1029/2025GL118344

Schuur, E. A., Abbott, B. W., Commane, R., Ernakovich, J., Euskirchen, E., Hugelius, G., ... & Turetsky, M. (2022). Permafrost and climate change: carbon cycle feedbacks from the warming Arctic. *Annual Review of Environment and Resources, 47*(1), 343-371. https://doi.org/10.1146/annurev-environ-012220-011847

Schuur, E. A., McGuire, A. D., Schädel, C., Grosse, G., Harden, J. W., Hayes, D. J., ... & Vonk, J. E. (2015). Climate change and the permafrost carbon feedback. *Nature, 520*(7546), 171-179. https://doi.org/10.1038/nature14338

Shur, Y., Jones, B. M., Jorgenson, M. T., Kanevskiy, M. Z., Liljedahl, A., Walker, D. A., Ward Jones, M. K., Fortier, D., & Vasiliev, A. (2025). Formation of Low-Centered Ice-Wedge Polygons and Their Orthogonal Systems: A Review. *Geosciences, 15*(7), 249. https://doi.org/10.3390/geosciences15070249

Shur, Y. L., & Jorgenson, M. T. (2007). Patterns of permafrost formation and degradation in relation to climate and ecosystems. *Permafrost and Periglacial Processes, 18*(1), 7-19. https://doi.org/10.1002/ppp.582

Smith, S. L., O’Neill, H. B., Isaksen, K., Noetzli, J., & Romanovsky, V. E. (2022). The changing thermal state of permafrost. *Nature Reviews Earth & Environment, 3*(1), 10-23. https://doi.org/10.1038/s43017-021-00240-1

Teltewskoi, A., Beermann, F., Beil, I., Bobrov, A., De Klerk, P., Lorenz, S., Lorenz, S., Lüder, A., Michaelis, D., & Joosten, H. (2016). 4000 years of changing wetness in a permafrost polygon peatland (Kytalyk, NE Siberia): A comparative high-resolution multi-proxy study. *Permafrost and Periglacial Processes, 27*(1), 76-95. https://doi.org/10.1002/ppp.1869

Treat, C. C., Jones, M. C., Camill, P., Gallego-Sala, A., Garneau, M., Harden, J. W., ... & Väliranta, M. (2016). Effects of permafrost aggradation on peat properties as determined from a pan-Arctic synthesis of plant macrofossils. *Journal of Geophysical Research: Biogeosciences, 121*(1), 78-94. https://doi.org/10.1002/2015JG003061

Treat, C. C., & Jones, M. C. (2018). Near-surface permafrost aggradation in Northern Hemisphere peatlands shows regional and global trends during the past 6000 years. *The Holocene, 28*(6), 998-1010. https://doi.org/10.1177/0959683617752858

Treat, C. C., Jones, M. C., Alder, J., Sannel, A. B. K., Camill, P., & Frolking, S. (2021). Predicted vulnerability of carbon in permafrost peatlands with future climate change and permafrost thaw in Western Canada. *Journal of Geophysical Research: Biogeosciences*, *126*(5), e2020JG005872. https://doi.org/10.1029/2020JG005872

Turunen, J., Tomppo, E., Tolonen, K., & Reinikainen, A. (2002). Estimating carbon accumulation rates of undrained mires in Finland–application to boreal and subarctic regions. *The Holocene, 12*(1), 69-80. https://doi.org/10.1191/0959683602hl522rp

van Dijk, E. J., Jungclaus, J., Sigl, M., Timmreck, C., & Krüger, K. (2024). High-frequency climate forcing causes prolonged cold periods in the Holocene. *Communications Earth & Environment, 5*(1), 242. https://doi.org/10.1038/s43247-024-01380-0

Vallerand, J., de Vernal, A., & Roy, N. (2024). Climate variations in eastern Hudson Bay over the past 3000 years. *Quaternary Science Reviews, 339,* 108862. https://doi.org/10.1016/j.quascirev.2024.108862

Vallée, S., & Payette, S. (2004). Contrasted growth of black spruce (Picea mariana) forest trees at treeline associated with climate change over the last 400 years. *Arctic, Antarctic, and Alpine Research, 36*(4), 400-406. https://doi.org/10.1657/1523-0430(2004)036[0400:CGOBSP]2.0.CO;2

Vardy, S. R., Warner, B. G., & Asada, T. (2005). Holocene environmental change in two polygonal peatlands, south-central Nunavut, Canada. *Boreas, 34*(3), 324-334. https://doi.org/10.1111/j.1502-3885.2005.tb01104.x

Watmough, S., Gilbert-Parkes, S., Basiliko, N., Lamit, L. J., Lilleskov, E. A., Andersen, R., ... & Zahn, G. (2022). Variation in carbon and nitrogen concentrations among peatland categories at the global scale. PLoS One, 17(11), e0275149. https://doi.org/10.1371/journal.pone.0275149

Webb, E. E., Liljedahl, A. K., Cordeiro, J. A., Loranty, M. M., Witharana, C., & Lichstein, J. W. (2022). Permafrost thaw drives surface water decline across lake-rich regions of the Arctic. *Nature Climate Change, 12*(9), 841-846. https://doi.org/10.1038/s41558-022-01455-w

Wickland, K. P., Jorgenson, M. T., Koch, J. C., Kanevskiy, M., & Striegl, R. G. (2020). Carbon dioxide and methane flux in a dynamic Arctic tundra landscape: Decadal-scale impacts of ice wedge degradation and stabilization. *Geophysical Research Letters, 47*(22), e2020GL089894. https://doi.org/10.1029/2020GL089894

Wolter, J., Lantuit, H., Fritz, M., Macias-Fauria, M., Myers-Smith, I., & Herzschuh, U. (2016). Vegetation composition and shrub extent on the Yukon coast, Canada, are strongly linked to ice-wedge polygon degradation. *Polar Research, 35(*1), 27489. https://doi.org/10.3402/polar.v35.27489

Wolter, J., Lantuit, H., Wetterich, S., Rethemeyer, J., & Fritz, M. (2018). Climatic, geomorphologic and hydrologic perturbations as drivers for mid-to late Holocene development of ice-wedge polygons in the western Canadian Arctic. *Permafrost and Periglacial Processes, 29*(3), 164-181. https://doi.org/10.1002/ppp.1977

Young, D. M., Baird, A. J., Charman, D. J., Evans, C. D., Gallego-Sala, A. V., Gill, P. J., Hughes, P. D. M., Morris, P. J., & Swindles, G. T. (2019). Misinterpreting carbon accumulation rates in records from near-surface peat. *Scientific reports, 9*(1), 17939. https://doi.org/10.1038/s41598-019-53879-8

Young, D. M., Baird, A. J., Gallego-Sala, A. V., & Loisel, J. (2021). A cautionary tale about using the apparent carbon accumulation rate (aCAR) obtained from peat cores. *Scientific Reports*, *11*(1), 9547. https://doi.org/10.1038/s41598-021-88766-8

Zhang, Y., Li, J., Wang, X., Chen, W., Sladen, W., Dyke, L., Dredge, L., Poitevin, J., McLennan, D., Steward, H., Kowalchuk, S., Wu, W., Kershaw, G. P., & Brook, R. K. (2012). Modelling and mapping permafrost at high spatial resolution in Wapusk National Park, Hudson Bay Lowlands. *Canadian Journal of Earth Sciences, 49*(8), 925-937. https://doi.org/10.1139/e2012-031

Zoltai, S. C., & Tarnocai, C. (1975). Perennially frozen peatlands in the western Arctic and Subarctic of Canada. *Canadian Journal of Earth Sciences, 12*(1), 28-43. https://doi.org/10.1139/e75-004

Table 1. Detailed results of the AMS radiocarbon dating of the basal ages (excluding the paleoreconstruction sites): uncalibrated ^{14}C age and calibrated 2-sigma range and median age. The calibration was performed using OxCal v4.4 (Ramsey, 2009) and the IntCal20 calibration curve (Reimer et al., 2020).

					Calibrated dates	
Site	**Depth (cm)**	**Lab ID**	**Dated material**	**Age (^{14}C yr BP)**	**2σ range (cal BP)**	**median (cal BP)**
Polygonal peatlands						
IW4	91–92	UOC-27860	Bulk peat	3030 ± 30	3083–3346	3215
SBF1	125–126	UOC-29266	Wood fragments	3360 ± 20	3492–3684	3588
SKID1	77–78	UOC-29268	Wood fragments	1580 ± 20	1401–1518	1460
Treed peat plateaus						
LSW9	71–72	UOC-30617	Bulk peat	1840 ± 35	1632–1825	1729
LSW10	65–66	UOC-29263	Bulk peat	365 ± 15	324–489	407
SLF5	75–76	UOC-28051	Coniferous needles	1110 ± 15	957–1058	1008
1994B-TB	262–263	UOC-30614	Bulk peat	5190 ± 35	5900–6103	6002
Permafrost fens						
PF5	57–58	UOC-28045	*Juncus* seeds	2090 ± 15	1997–2109	2053
Non-permafrost fens						
SSF11	23–24	UOC-27342	Bulk peat	1560 ± 20	1377–1515	1446
PF12	50–51	UOC-27861	Wood fragments	2160 ± 30	2006–2305	2156
LMF6	36–37	UOC-28047	Wood fragments	1280 ± 15	1177–1276	1227
HLG-1	47–48	UOC-29267	Bulk peat	1270 ± 15	1130–1274	1202
SLF4	36–37	UOC-28050	Bulk peat	2490 ± 20	2492–2713	2603
Coastal fens						
CF7	26–27	UOC-28048	Wood fragments	120 ± 15	30–259	145
CF8	36–37	UOC-28049	Moss stems, seeds	110 ± 15	33–257	145

Table 2. Distance from the coast, peat thickness, basal age, total carbon mass, peat accumulation rate (PAR), and long-term rate of carbon accumulation (LORCA) for all study sites. PAR (mm a^{-1}) and LORCA (g C m^{-2} a^{-1}) were calculated by dividing the peat thickness and total C mass by the ^{14}C calibrated median age. *Sites for detailed paleoecological reconstructions.

Site name	Distance to coast (km)	Peat thickness (cm)	Basal age (cal BP)	PAR (mm a^{-1})	Total C mass (kg C m^{-2})	LORCA (g C m^{-2} a^{-1})
Polygonal peatlands						
WAP05B*	13.5	110	2391	0.46	75.0	31.4
WAP34A*	46.8	180	3542	0.51	94.2	26.6
Owl 2.1*	38.9	165	3707	0.45	70.4	19.0
IW1*	26.8	105	3588	0.29	45.1	12.6
IW4	25.4	94	3215	0.29	44.0	13.7
SBF1	43.4	126	3588	0.35	67.2	18.7
SKID1	36.6	78	1460	0.53	46.7	32.0
Treed peat plateaus						
LSW9	13.8	72	1729	0.42	37.1	21.4
LSW10	9.2	66	407	1.62	36.0	88.4
SLF5	25.6	76	1008	0.75	37.2	36.9
WAP27-1B*	78.1	251	5706	0.44	124.7	21.9
1994B-TB	76.9	263	6002	0.44	123.5	20.6
Permafrost fens						
PF5	14.7	58	2053	0.28	32.3	15.7
Non-permafrost fens						
SSF11	11.4	24	1446	0.17	15.0	10.4
PF12	18.6	51	2156	0.24	25.8	12.0
LMF6	13.7	38	1227	0.31	19.1	15.6
HLG-1	15.2	51	1202	0.42	20.6	17.2
SLF4	76.4	37	2603	0.14	21.5	8.2
Coastal fens						
CF7	0.8	27	145	1.86	10.4	71.9
CF8	0.9	37	145	2.55	16.4	113.3

Table 3. Detailed AMS radiocarbon dating results for paleo-reconstruction sites: ^{14}C age (uncalibrated), 2-sigma range and median age (calibrated using OxCal v4.4 (Ramsey, 2009) and the IntCal20 calibration curve (Reimer et al., 2020)), and modelled dates (with 95% confidence interval range) from the *Bacon* age-depth models.

Site	Depth (cm)	Lab ID	Dated material	Calibrated dates			Modelled dates	
				Age (^{14}C yr BP)	2σ range (cal BP)	median (cal BP)	range (cal BP)	median (cal BP)
WAP05B	13–14	UOC-28619	Moss stems, Ericaceae leaves	95 ± 15	34–255	145	33–257	133
	46–47	UOC-26525	Ericaceae leaves, moss stems, Cyperaceae seeds	1080 ± 15	929–978	954	892–1046	966
	84–85	UOC-28620	Moss stems	2000 ± 20	1879–1991	1935	1823–1990	1919
	109–110	UOC-26524	Ericaceae leaves, moss stems	2390 ± 15	2346–2436	2391	2333–2535	2389
IW1	9–10	UOC-30226	*Sphagnum* stems	1180 ± 30	993–1179	1086	764-1123	980
	27–28	UOC-30227	*Sphagnum* stems	1270 ± 30	1078–1283	1181	1153-1351	1252
	60–61	UOC-30228	*Sphagnum* stems	2240 ± 30	2150–2339	2245	2101-2353	2212
	84–85	UOC-30229	Wood fragments	2540 ± 30	2496–2745	2621	2531-2813	2706
	104–105	UOC-28046	Wood fragments	3360 ± 20	3492–3684	3588	3457-3686	3565
WAP34A	16–17	UOC-29257	*Sphagnum* stems	320 ± 20	309–447	378	279–455	370
	42–43	UOC-28624	*Sphagnum* stems, *Picea* needles	1400 ± 15	1289–1344	1317	956–1345	1293
	110–111	UOC-26522	*Sphagnum* stems	1870 ± 15	1727–1825	1776	1729–2072	1806
	156–157	UOC-29258	Wood, *Larix* needles	2940 ± 20	3004–3165	3085	2958–3179	3081
	179–180	UOC-26523	Bulk peat	3350 ± 15	3490–3594	3542	3479–3670	3562
WAP34B	87–88	UOC-26532	*Sphagnum* stems, Ericaceae leaves	645 ± 20	559–594	577	NA	NA
OWL 2.1	5–6	UOC-29260	*Sphagnum* stems	75 ± 15	40–254	147	15–109	41
	20–21	UOC-26526	*Sphagnum* stems	150 ± 15	62–118	90	162–277	246
	36–37	UOC-26527	Moss stems, *Sphagnum* stems	1680 ± 15	1531–1597	1564	1404–1601	1543
	84–85	UOC-28622	Ericaceae leaves, *Picea* needles, *Sphagnum* stems	2170 ± 15	2105–2300	2203	2019–2280	2132
	141–142	UOC-26528	*Sphagnum* stems	2470 ± 15	2631–2703	2667	2575–2710	2664
	165–166	UOC-26529	Moss stems, Ericaceae leaves	3460 ± 15	3684–3729	3707	3584–3802	3684
WAP27-1B	6–7	UOC-29259	*Sphagnum* stems, Ericaceae leaves	60 ± 15	41–250	146	10–141	49
	43–44	UOC-25971	Charcoal	850 ± 20	721–787	754	676–781	729
	129–130	UOC-25972	*Sphagnum* stems	1610 ± 25	1431–1534	1483	1412–1572	1496
	143–144	UOC-25973	*Sphagnum* stems	1750 ± 20	1575–1705	1640	1590–1792	1665
	164–165	UOC-25974	Charcoal	2670 ± 25	2746–2786	2766	2678–2837	2750

188–189	UOC-28621	*Sphagnum* stems	3380 ± 20	4242–4407	4325	3491–3694	3594
250–251	UOC-25975	Ericaceae leaves, moss stems, Cyperaceae seeds	5010 ± 25	5656–5755	5706	5593–5870	5702

Table 4. Peat and carbon accumulation rates (PAR; CAR), and median N% and C/N ratios for the zones identified using CONISS hierarchical clustering. PAR (mm a^{-1}) was calculated by dividing the zone thickness by its deposition time obtained from the *Bacon* age-depth models. Similarly, CAR (g C m^{-2} a^{-1}) was calculated by dividing the carbon mass in a zone by its deposition time. Periods (cal BP) are median ages obtained from *Bacon* models.

Site	Zone	Depth (cm)	Period (cal BP)	Vegetation	PAR (mm a^{-1})	CAR (g C m^{-2} a^{-1})	N% Median	C/N ratio Median
WAP05B	1	109–89	2373–2014	*Tomentypnum nitens*	0.56	32.1	2.10	19.5
	2a	89–52	1998–1121	Calliergonaceae	0.42	25.1	2.26	18.0
	2b	52–16	1095–209	Calliergonaceae, *Carex* spp.	0.41	32.3	2.42	17.9
	3	16–0	173–present	*Dicranum spp.*, Ericaceae	0.67	51.9	0.94	45.9
IW1	1	105–83	3565–2681	Mosses, *Picea mariana*	0.25	13.0	NA	NA
	2	83–59	2656–2184	*Sph. fuscum, Picea mariana*	0.51	15.8	NA	NA
	3a	59–46	2157–1775	*Picea mariana*	0.34	19.8	NA	NA
	3b	46–6	1743–800	*Sph. fuscum, Picea mariana*	0.42	15.8	NA	NA
	3c	0–6	738–present	Lichens, Ericaceae	0.07	4.6	NA	NA
WAP34A	1a	180–159	3562–3150	*Carex* spp., *Larix laricina*	0.51	33.0	2.76	14.3
	1b	159–104	3128–1766	*Larix laricina, Picea* spp.	0.40	28.3	1.77	25.2
	2a	104–66	1759–1468	*Sph. fuscum* type, *V. oxycoccos*	1.31	43.4	0.45	94.8
	2b	66–23	1460–581	*Sph. fuscum* type*, Picea* spp.	0.49	20.8	0.52	85.1
	2c	23–0	549–present	*Dicranum* spp., *Sph. lenense*	0.37	19.6	1.05	41.3
OWL2.1	1a	165–144	3693–2722	Brown mosses, Cyperaceae	0.23	13.2	2.36	16.3
	1b	92–144	2707–2208	*S.* sect. *Acutifolia, V. oxycoccos*	1.04	30.6	0.67	64.5
	2a	92–26	2198–516	*Sphagnum* spp., *Picea* spp.	0.39	18.9	1.26	37.0
	2b	26–0	411–present	*Sphagnum lenense*	0.55	22.0	0.53	78.5
WAP271B	1a	251–194	5702–3793	*Carex* spp., *L. laricina,* Betulaceae	0.30	19.5	2.36	18.7
	1b	194–161	3763–2627	*Picea* spp.*, S.* sect. *Acutifolia*	0.29	18.3	0.83	55.7
	1c	161–139	2584–1608	*Sph. fuscum, Picea* spp.	0.23	9.7	0.70	68.2
	2	139–49	1596–788	*S.* sect. *Cuspidata, V. oxycoccos*	1.11	45.4	0.70	63.4
	3a	49–5	781–36	*Sph. fuscum, Picea* spp.	0.59	24.9	0.50	87.8
	3b	5–0	16–present	Lichens, *Rhododendron* sp.	0.62	25.4	1.06	43.3

Table 5. Peatland basal age (calibrated median age), total carbon mass (kg C m^{-2}), and the timing of permafrost aggradation in the paleoreconstruction sites across low Arctic and subarctic tundra and northern boreal forest.

	WAP05	IW1	WAP34	OWL 2.1	WAP27-1B
Vegetation zone	Lowarctic	Subarctic	Subarctic	Subarctic	Boreal
Latitude	58.34	58.29	58.05	57.71	57.61
Ecosystem type	Polygonal peatland	Polygonal peatland	Polygonal peatland	Polygonal peatland	Treed plateau bog
Basal age (cal BP)	2390	3565	3560	3685	5700
Total C mass (kg m^{-2})	75.0	45.1	94.2	70.4	124.7
Permafrost aggradation (cal BP)	~1100-200	~1050	~1300-1200	~1500	~2590–1760 ~760

Supplementary material to

Polygonal peatlands and treed plateau bog in Northwest Hudson Bay Lowlands, Canada: Holocene development and permafrost dynamics

Tiina H. M. Kolari, Laure Gandois, Frédéric Bouchard, Alison E. Cassidy, Nicole K. Sanderson, Rémi Tremouille, Julien Arsenault, Maialen Barret, Adam Collingwood, Lucile Cosyn Wexteen, Sylvain Ferrant, LeeAnn Fishback, Karen Richardson, & Michelle Garneau

CONTENT

1 Peat coring locations

Table S1. Peat coring locations in Wapusk National Park (WNP) and the Churchill Wildlife Management Area. At the WAP34 site, a peat profile was collected from both the polygon centre (A) and the ice wedge rim (B). Ecosystem types roughly correspond to the CaMP peatland categories (The Canadian Model for Peatlands; Bona et al., 2020). Ecotypes are described in the Wapusk Ecotype Mapping report by Pomonorenko et al. (2014). Sites PF5 and P12 are open fens characterized by moss *Scorpidium scorpioides*, which are usually considered as moderately rich fens. In the Ecotype Mapping Report (Pomonororenko et al., 2014), these fens fall into the description of poor sedge fens. *Vegetation zones: LAST = Low Arctic Shrub Tundra, SWT = Subarctic Woodland Tundra, NBW = Northern Boreal Woodland (Baldwin et al., 2019). **Bioclimatic zones for sites in WNP: LHT = Low Hypoarctic Tundra, S = Subarctic, HBW = High Boreal Woodland (Pomonorenko et al., 2014).

No.	Site name	Date (dd/mm/yyyy)	Lat.	Long.	Vegetation zone*	Bioclimatic zone**	Distance to the coast (km)	Ecosystem type	Ecotype
	Paleoreconstruction sites								
1	WAP05B	10/08/2023	58.343073	-93.269232	LAST	LHT	13.5	Polygonal peatland	Shrub moss lichen
2	WAP34 (A and B)	12/08/2023	58.046339	-93.658058	SWT	S	46.8	Polygonal peatland	Lichen dwarf shrub
3	Owl 2.1	14/08/2023	57.710350	-93.361020	SWT	S	38.9	Polygonal peatland	Lichen dwarf shrub
4	IW1	17/07/2024	58.288903	-93.473413	SWT	S	26.8	Polygonal peatland	Lichen dwarf shrub
5	WAP27-1B	15/08/2023	57.610471	-93.991276	NBW	-	78.1	Treed peat plateau bog	Lichen spruce woodland
	Other permafrost sites								
6	PF5	18/07/2024	58.154935	-93.152418	SWT	S	14.7	Open rich fen	Poor sedge fen
7	IW4	17/07/2024	58.294493	-93.452422	SWT	S	25.4	Polygonal peatland	Lichen dwarf shrub
8	SBF1	19/08/2024	57.882780	-93.513150	SWT	S	43.4	Polygonal peatland	Lichen dwarf shrub
9	SKID1	20/03/2025	57.848140	-93.381710	SWT	S	36.6	Polygonal peatland	Shrub moss lichen
10	LSW9	17/08/2025	57.751970	-92.944020	SWT	S	13.8	Treed peat plateau bog	Lichen spruce woodland
11	SLF5	21/08/2024	58.496550	-93.643040	SWT	HBW	25.6	Forested peat plateau bog	Spruce larch forest
12	LSW10	19/07/2024	57.588435	-92.737215	SWT	HBW	9.2	Forested peat plateau bog	Lichen spruce woodland
13	1994B-TB	13/08/2025	57.510230	-93.902530	NBW	HBW	76.9	Treed peat plateau bog	Spruce larch forest
	Non-permafrost fens								
14	CF7	18/07/2024	58.134033	-92.864107	SWT	LHT	0.8	Open rich fen	Coastal fen
15	CF8	18/07/2024	58.133262	-92.865413	SWT	LHT	0.9	Open rich fen	Coastal fen
16	SSF11	20/07/2024	58.142019	-93.078173	SWT	S	11.4	Open poor fen	Shrub-sedge fen
17	PF12	20/07/2024	58.161156	-93.229280	SWT	S	18.6	Open rich fen	Poor sedge fen
18	LMF6	18/07/2024	58.169440	-93.144633	SWT	S	13.7	Treed rich fen	Larch moss fen
19	HLG-1	18/03/2025	58.623072	-93.813732	SWT	-	15.2	Open rich fen	Poor sedge fen

20	SLF4	19/08/2024	57.531930	-93.910830	NBW	HBW	76.4	Treed rich fen	Spruce larch forest

2 Photographs of permafrost peat cores from paleoreconstruction sites

Figure S1. Peat profile collected from the lowarctic polygonal peatland WAP05B.

Figure S2. Peat profile collected from the subarctic polygonal peatland IW1.

Figure S3. Peat profile collected from the subarctic polygonal peatland WAP34A.

Figure S4. Peat profile collected from the subarctic polygonal peatland OWL 2.1.

Figure S5. Peat cores collected from the northern boreal treed peat plateau WAP27-1B.

3 Age-depth models for the paleoreconstruction sites

Age-depth models were built using the R package *rbacon* version 3.5.2 (Blaauw & Christen, 2011) and the IntCal20 calibration curve (Reimer et al., 2020). The surface of the peat profile was set at -73 or -74, corresponding to 2023 or 2024 when the profile was collected, with 0 representing 1950 CE. The blue violin plots represent the ^{14}C dates with confidence intervals. The red line represents the mean model, and the grey dashed lines show the 95% confidence intervals. In the small panels above, the green lines represent the prior distributions, and the grey plots show the posterior distributions. None of the prior values were modified.

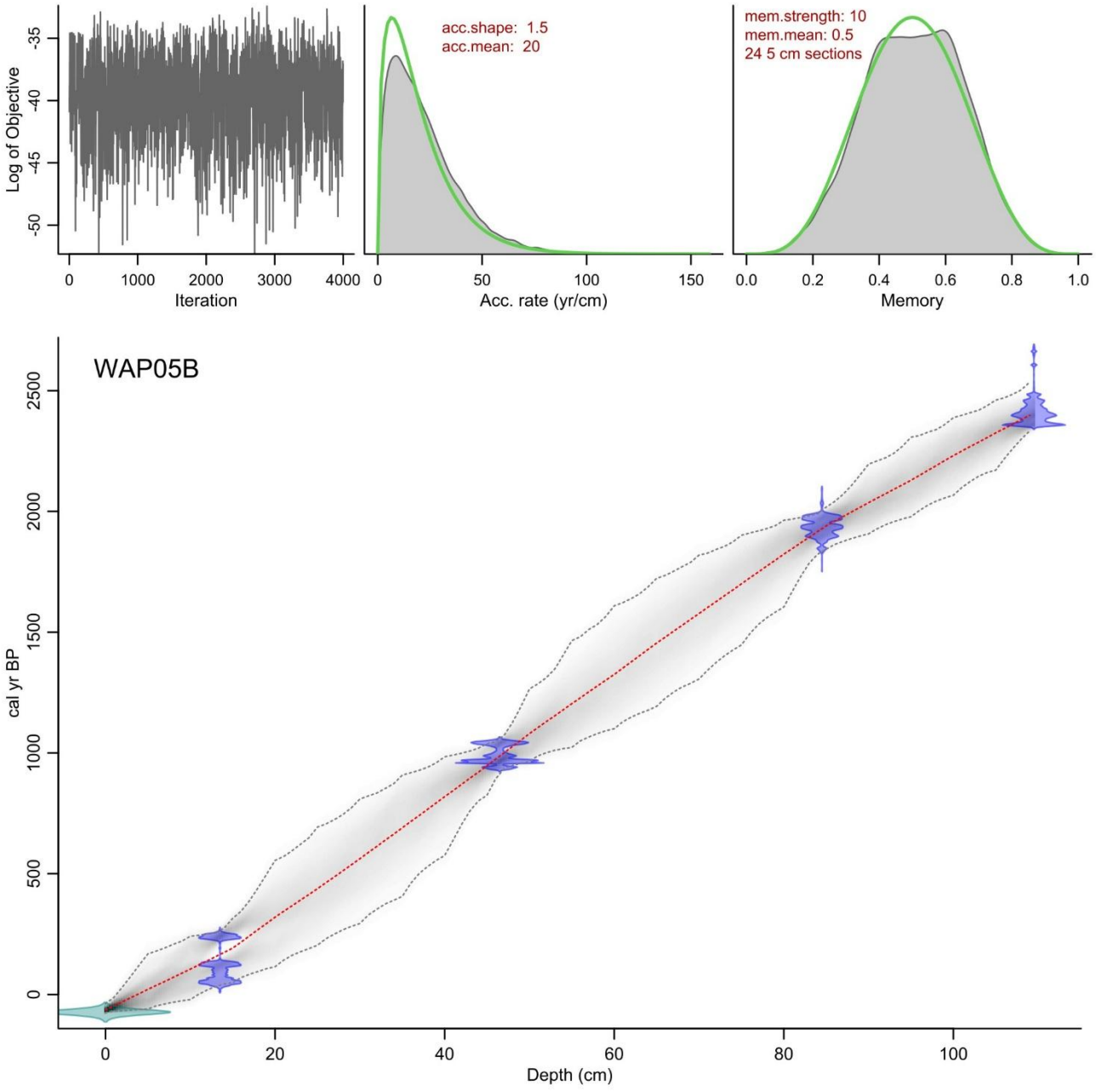

Figure S6. Age-depth model for the lowarctic polygonal peatland WAP05B.

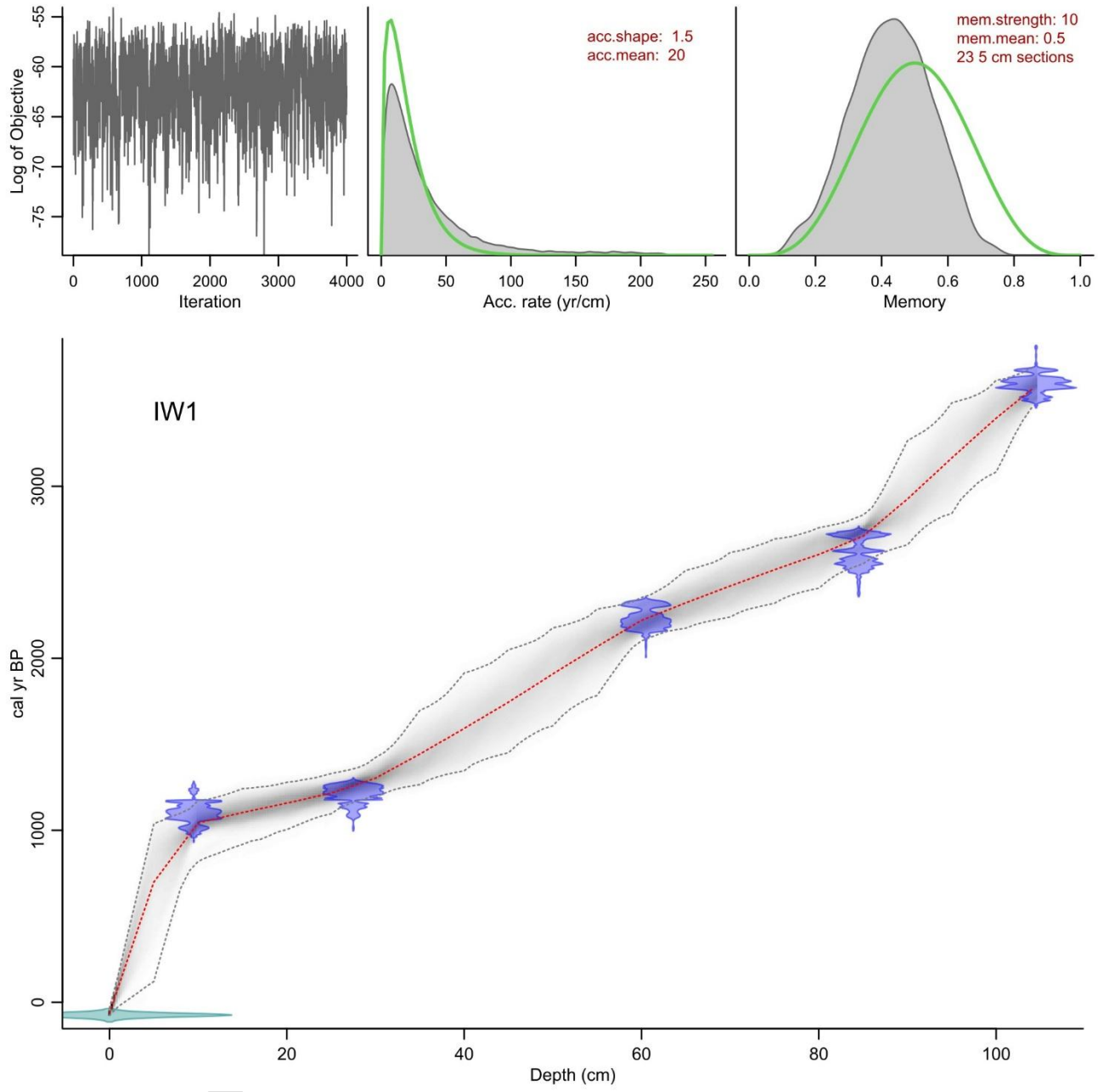

Figure S7. Age-depth model for the subarctic polygonal peatland IW1.

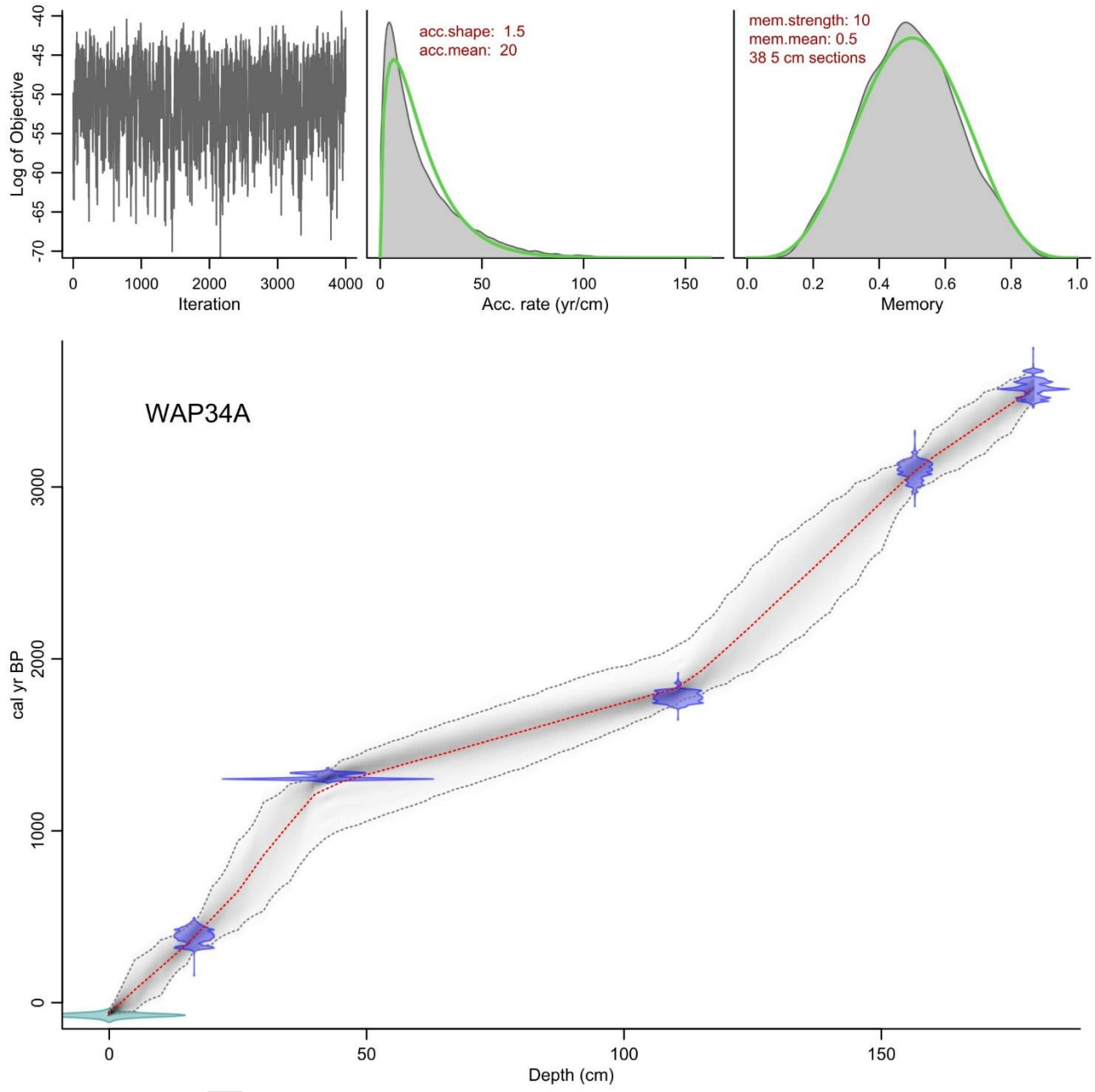

Figure S8. Age-depth model for the subarctic polygonal peatland WAP34A.

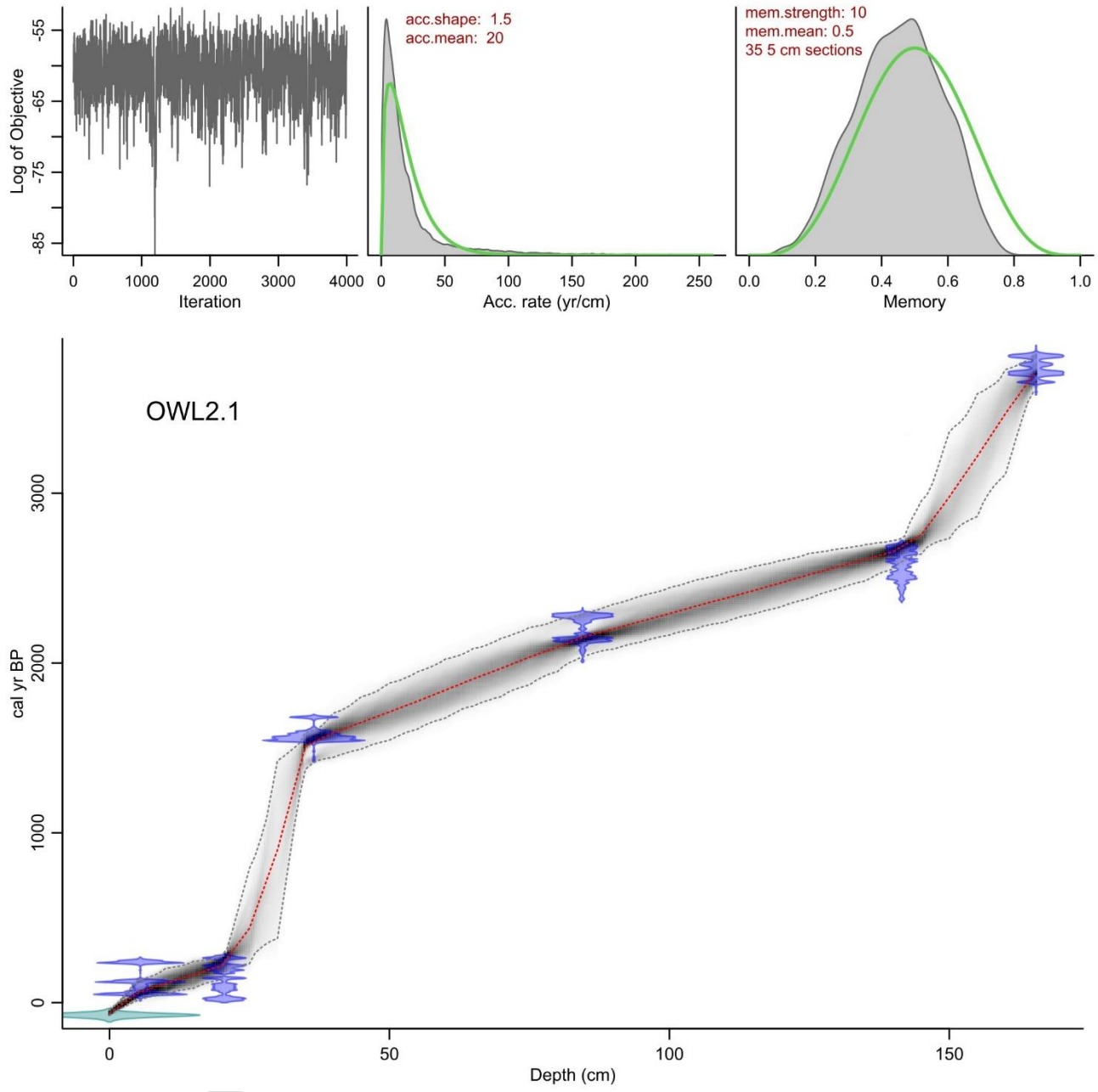

Figure S9. Age-depth model for the subarctic polygonal peatland OWL 2.1.

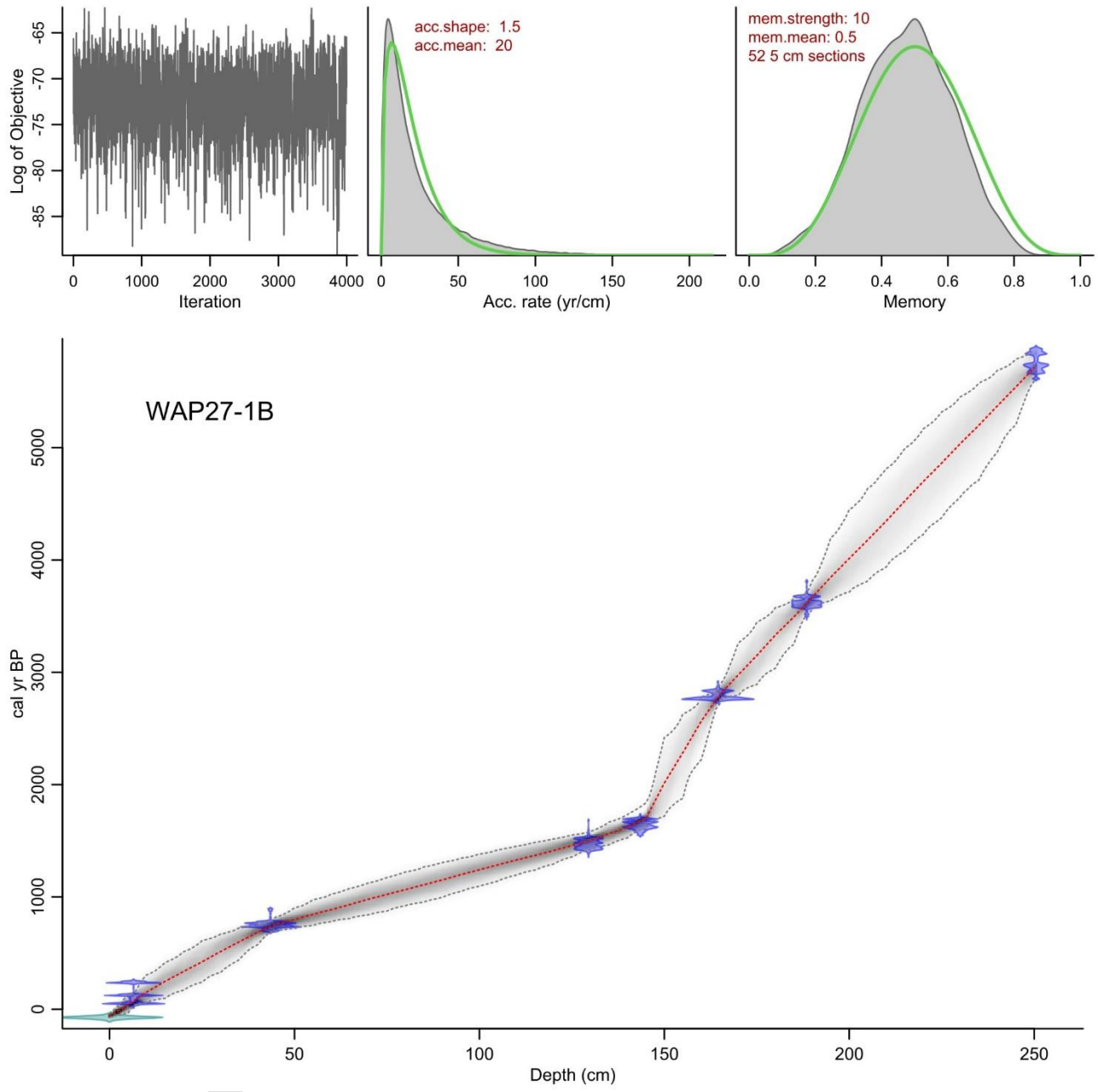

Figure S10. Age-depth model for the treed peat plateau WAP27-1B.

4 Ranges for peat accumulation rate (PAR) and long-term apparent rate of carbon accumulation (LORCA)

Table S2. Ranges for peat accumulation rate (PAR; mm a^{-1}) and long-term apparent rate of carbon accumulation (LORCA, g C m^{-2} a^{-1}), calculated using the entire age probability ranges (2σ range (cal BP)). PAR and LORCA were calculated by dividing the peat thickness and total carbon mass by the basal age, respectively.

			Calibrated dates					
Site name	Peat thickness (cm)	Total C mass (kg C m^{-2})	Lab ID	Depth (cm)	2σ range (cal BP)	Probability (%)	PAR (mm a^{-1})	LORCA (g C m^{-2} a^{-1})
WAP05B*	110	75.0	UOC-26524	109–110	2346–2436	91.5	0.45–0.47	30.8–31.9
WAP34A*	180	94.2	UOC-26523	179–180	3490–3594	76.7	0.50–0.52	26.2–27.0
Owl 2.1*	165	70.4	UOC-26529	164–165	3684–3729	41.4	0.44–0.45	18.8–19.1
IW1*	105	45.1	UOC-28046	104–105	3492–3684	95.4	0.29–0.30	12.2–12.9
IW4	94	44.0	UOC-27860	91–92	3083–3346	95.4	0.28–0.30	13.1–14.3
SBF1	126	67.2	UOC-29266	125–126	3492–3684	95.4	0.34–0.36	18.3–19.3
SKID1	78	46.7	UOC-29268	77–78	1401–1518	95.4	0.51–0.56	30.6–33.3
LSW9	72	37.1	UOC-30617	71–72	1632–1825	95.4	0.39–0.44	20.3–22.7
LSW10	66	36.0	UOC-29263	65–66	324–489	95.4	1.35–2.04	73.6–111.1
SLF5	76	37.2	UOC-28051	75–76	957–1058	95.4	0.72–0.79	35.2–38.8
WAP27–1B*	251	124.7	UOC-25975	250–251	5656–5755	69.1	0.44–0.44	21.7–22.0
1994B–TB	263	123.5	UOC-30614	262–263	5900–6103	95.4	0.43–0.45	20.2–20.9
PF5	58	32.3	UOC-28045	57–58	1997–2109	95.4	0.28–0.29	15.3–16.2
SSF11	24	15.0	UOC-27342	23–24	1377–1515	95.4	0.16–0.17	9.9–10.9
PF12	51	25.8	UOC-27861	50–51	2006–2305	95.4	0.22–0.25	11.2–12.9
LMF6	38	19.1	UOC-28047	36–37	1177–1274	95.4	0.30–0.32	15.0–16.2
HLG–1	51	20.6	UOC-29267	47–48	1130–1274	95.4	0.40–0.45	16.2–18.3
SLF4	37	21.5	UOC-28050	36–37	2492–2713	95.4	0.14–0.15	7.9–8.6
CF7	27	10.4	UOC-28048	26–27	30–259	95.4	1.04–9.00	40.3–347.5
CF8	37	16.4	UOC-28049	36–37	33–257	95.4	1.44–11.21	63.9–497.8

5 Ranges for peat accumulation rate (PAR) at the paleoreconstruction sites

Table S3. 95% confidence intervals from the Bacon age-depth models for the start and the end of each zone identified by CONISS clustering of the plant macrofossil data. Ranges for peat accumulation rate (PAR; mm a^{-1}) and carbon accumulation rate (CAR; g C m^{-2} a^{-1}) were calculated using the entire age probability ranges (95% confidence intervals).

			Period (cal BP)			
Site	**Zone**	**Depth (cm)**	**Start**	**End**	**CAR (g C m^{-2} a^{-1})**	**PAR (mm a^{-1})**
WAP05B	1	109–89	2508–2299	2151–1898	28.6–32.6	0.50–0.57
	2a	89–52	2108–1888	1312–1001	24.8–27.7	0.42–0.46
	2b	52–16	1286–988	345–70	30.4–31.2	0.38–0.39
	3	16–0	315–49	present (2023 CE)	32.6–107.8	0.42–1.39
IW1	1	105–83	3686–3457	2792–2511	12.1–12.8	0.23–0.25
	2	83–59	2780–2486	2329–2064	16.5–17.7	0.53–0.57
	3a	59–46	2316–2003	2065–1498	15.0–30.1	0.26–0.52
	3b	46–6	2050–1451	1058–310	13.1–15.0	0.35–0.40
	3c	0–6	1039–121	present (2024 CE)	3.3–19.1	0.05–0.31
WAP34A	1a	180–159	3670–3479	3277–3018	29.5–34.5	0.46–0.53
	1b	159–104	3233–3005	2000–1654	28.5–31.2	0.41–0.45
	2a	104–66	1991–1643	1634–1228	30.5–35.4	0.92–1.06
	2b	66–23	1625–1216	799–402	22.1–22.5	0.52–0.53
	2c	23–0	746–388	present (2023 CE)	14.7–26.0	0.28–0.50
OWL2.1	1a	166–144	3810–3595	2890–2633	13.4–14.0	0.23–0.24
	1b	92–144	2830–2621	2363–2102	29.5–32.7	1.00–1.11
	2a	92–26	2353–2092	863–292	17.6–21.3	0.37–0.44
	2b	26–0	791–230	present (2023 CE)	12.1–34.6	0.30–0.86
WAP271B	1a	251–194	5870–5593	4099–3629	18.9–21.0	0.29–0.32
	1b	194–161	4009–3620	2790–2336	16.2–17.1	0.26–0.27
	1c	161–139	2779–2223	1715–1517	8.9–13.4	0.21–0.31
	2	139–49	1699–1507	880–717	44.7–46.4	1.10–1.14
	3a	49–5	860–713	133 cal BP – 1985 CE	24.8–25.5	0.59–0.61
	3b	5–0	94 cal BP – 1991 CE	present (2023 CE)	15.8–64.3	0.38–1.56

6 Linear relationship of peat thickness, median age, and carbon mass to distance to coast

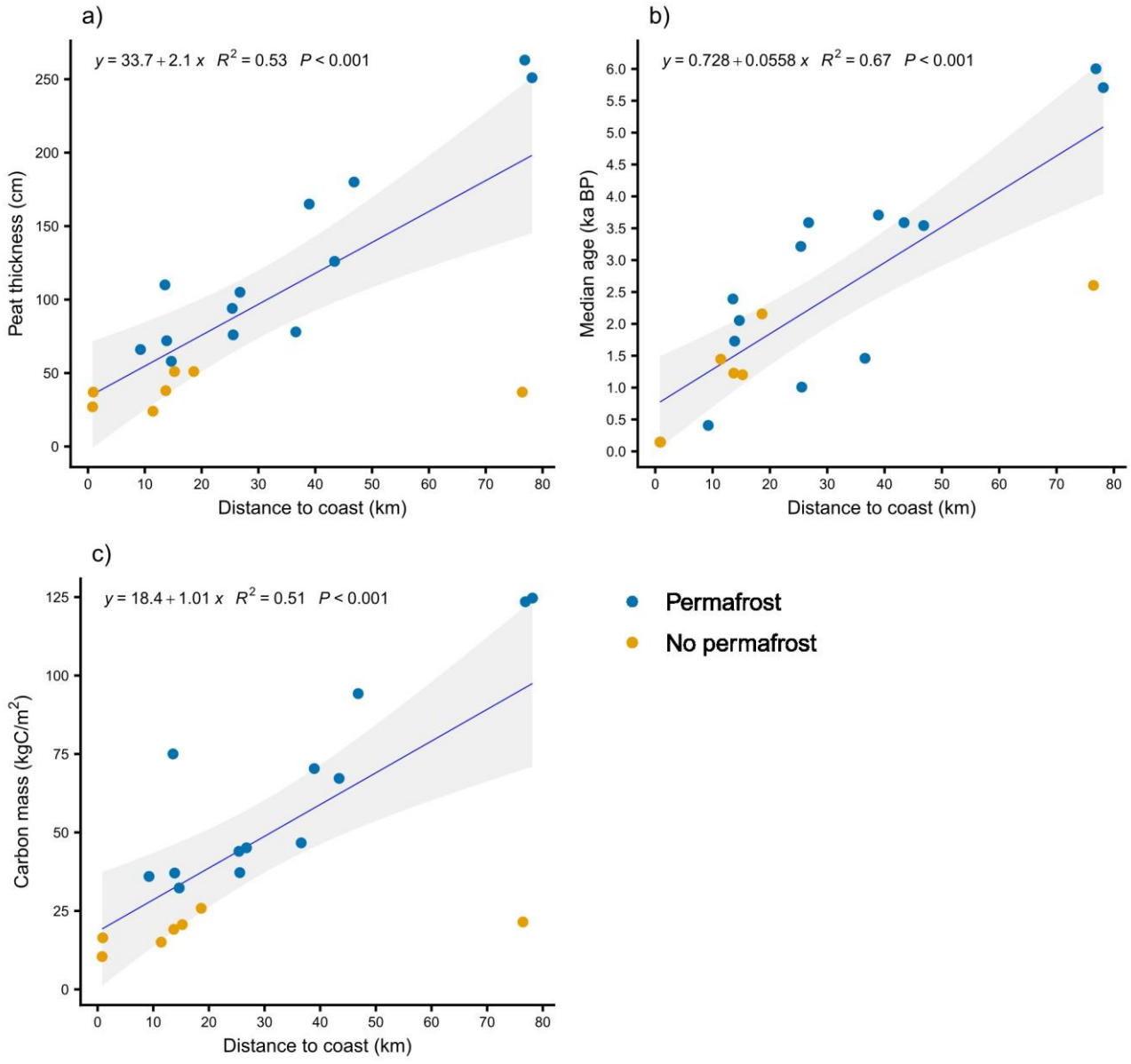

Figure S11. The linear relationship between distance to the coast (km) and a) peat thickness (cm), b) peatland age (ka cal BP), and c) carbon mass (kg C/m^2).

References

Baldwin, K., Allen, L., Basquill, S., Chapman, K., Downing, D., Flynn, N., MacKenzie, W., Major, M., Meades, W., Meidinger, D., Morneau, C., Saucier, J-P., Thorpe, J., Uhlig, P. (2019). Vegetation Zones of Canada: a Biogeoclimatic Perspective. [Map] Scale 1:5,000,000. *Natural Resources Canada, Canadian Forest Service. Great Lake Forestry Center, Sault Ste. Marie, ON, Canada*.

Blaauw, M. & Christen, J.A. (2011). Flexible paleoclimate age-depth models using an autoregressive gamma process. *Bayesian Analysis, 6*(3), 457-474. https://doi.org/10.1214/11-BA618

Bona, K. A., Shaw, C., Thompson, D. K., Hararuk, O., Webster, K., Zhang, G., Voicu, M., & Kurz, W. A. (2020). The Canadian model for peatlands (CaMP): A peatland carbon model for national greenhouse gas reporting. *Ecological Modelling, 431,* 109164. https://doi.org/10.1016/j.ecolmodel.2020.109164

Ponomarenko, S., Quirouette, J., Sharma, R. and D. McLennan. (2014). Ecotype Mapping Report for Wapusk National Park. Monitoring and Ecological Information. *Natural Resource Conservation. Parks Canada. Gatineau, QC, Canada*.

Reimer, P. J., Austin, W. E., Bard, E., Bayliss, A., Blackwell, P. G., Ramsey, C. B., Butzin, M., Cheng., H., Edwards, R. L., Friedrich, M., Grootes, P. M., Guilderson, T. P., Hajdas, I., Heaton, T. J., Hogg, A. G., Hughen, K. A., Kromer, B., Manning, S. W., Muscheler, R., Palmer, J. G., Pearson, C., van der Plicht, J., Reimer, R. W., Richards, D. A., Scott, E. M., Southon, J. R., Turney, C. S. M., Wacker, L., Adolphi, F., Büntgen, U., Capano, M., Fahrni, S. M., Fogtmann-Schultz, A., Friedrich, R., Köhler, P., Kudsk, S., Miyake, F., Olsen, J., Reinig, F., Sakamoto, M., Sookdeo, A., & Talamo, S. (2020). The IntCal20 Northern Hemisphere radiocarbon age calibration curve (0–55 cal kBP). Radiocarbon, 62(4), 725-757. https://doi.org/10.1017/RDC.2020.41